in the SC. These findings suggest that CS16 was more effective as a carrier for delivering BLM topically into the skin than C16 vesicles.

3.4. Permeation of CS16-vesicle through the skin observed by CLSM

The ability of CS16-vesicles to deliver encapsulated hydrophilic fluorescent probes into full-thickness skin was observed by CLSM. Sections of hairless rat skin were treated for 3 h with a topical preparation of CS16-vesicles labelled with DiI and entrapped with calcein (Fig. 8A); a mixture suspension of free calcein and DiI-labeled empty CS16-vesicles (Fig. 8B); and a mixture solution of free DiI and calcein as a control (Fig. 8C). When CS16-vesicles labelled with DiI and containing calcein were applied, the fluorescence of calcein appeared to be quite uniform and quite intense in the whole SC. Co-location of calcein and DiI, which produced a yellow colour, was observed extensively, even in the bottom of SC (Fig. 8A). However, a mixture of calcein and empty CS16-vesicles delivered less intense fluorescence when compared against the first formulation (Fig. 8A vs. B). Finally, from the mixture solution of free DiI and calcein, it could be clearly seen that fluorescence of lipophilic DiI was homogenously distributed across the SC and free calcein was unable to penetrate into the SC (Fig. 8C). This finding suggests that ultra-deformable vesicles could deliver hydrophilic drugs encapsulated in vesicles.

4. Discussion

We have already reported that BLM can be encapsulated in ultra-deformable vesicles composed of EPC and Cholate for topical application [10]. To enhance permeation of drug through skin, we developed a novel, ultra-deformable vesicle incorporating Sit-G, an effective absorption enhancer in intestinal and nasal mucosae [11,12].

In this study we report the efficacy of ultra-deformable formulations containing Sit-G and loaded with the candidate drug BLM. Penetration of lipid vesicles through skin is related to the deformability of the vesicle membrane and only optimized carriers can pass through pores smaller than their own diameter. Increasing the level of surfactant in vesicle membranes brings no advantages in terms of transcutaneous permeation efficiency above a certain concentration. Only an optimum ratio of lipid and surfactant could lead to bilayer flexibility liposomal membranes. Addition of other lipophilic compounds, such as cholesterol sulfate, to lipophilic/amphiphilic bilayers tend to decrease their elasticity, even at low molar concentrations of amphiphilic compounds in the bilayer [19].

To determine the amount of Sit-G incorporated into vesicles, we preliminarily measured the elasticity of preparations containing Tween or Cholate at different concentrations, plus Sit-G at 5% and 10% (w/w). Incorporation of 5% (w/w) Sit-G into Cholate formulations did not decrease their elasticity value (Fig. 2B), but incorporation of 10% (w/w) Sit-G significantly decreased it (data not shown). The absorption enhancing effect exerted by Sit-G could be attributed to its steroidal structure and similarity with cholesterol and Cholate. Incorporation of steroids in fluid vesicle bilayers enhances the degree in molecular ordering or change the compaction of bilayers [20]. Therefore, the addition of 5% (w/w) (6 mol%) Sit-G as a small amount to CS-vesicle bilayers was useful and did not decrease elasticity, but decreases in elasticity might become noticeable at high concentrations of Sit-G.

The strength of interaction between different surfactants in the bilayer was dependent on their molar ratios. At a high molar ratio, Cholate showed greater effect on J_{flux} than Tween, but this difference was limited because the hydrophile–lipophile balance (HLB) of Cholate and Tween was similar [8]. Maximum elasticity of C- and CS-vesicles was seen in 16% (w/w) Cholate, C16 and CS16 preparations. The elasticity of T-vesicles might increase with further addition of Tween, but too much surfactant might cause skin irritation as well as reducing drug entrapment by creating mixed micelles [21]. These mixed micelles have been reported to be less effective in transdermal drug delivery, as compared with ultra-deformable vesicles, because micelles are much less sensitive

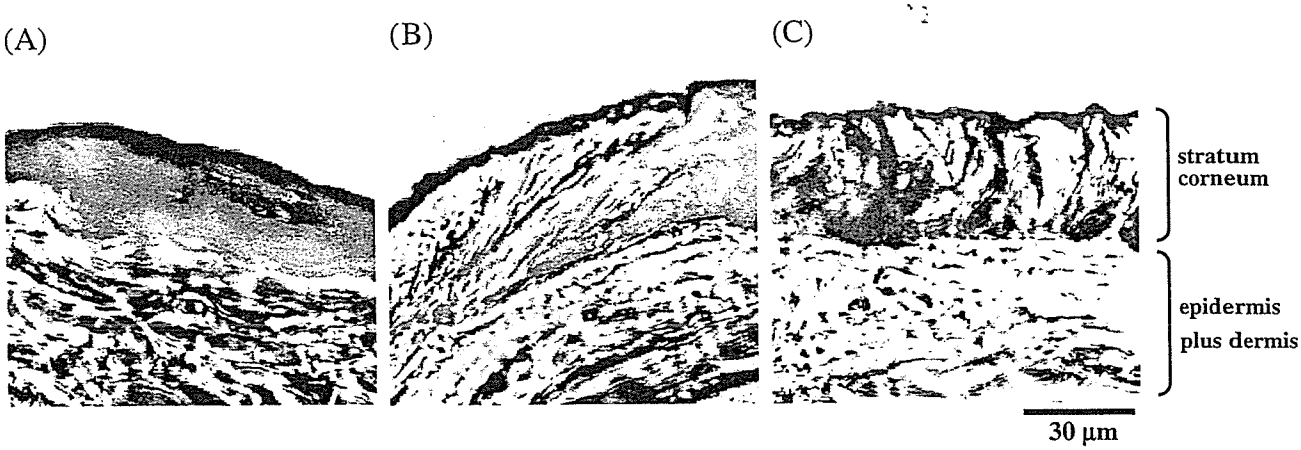

Fig. 8. Optical cross-sections perpendicular to the hairless rat surface incubated with fluorescent-labeled CS16-vesicles. Cross-sectional images were obtained by CLSM following a 3 h-application of CS16-vesicles labeled with DiI and entrapped with calcein (A), a mixture suspension of free calcein and CS16-vesicles labeled with DiI (B), and a mixture solution of free DiI and calcein in 5% ethanol solution (C).

to water activity gradients than ultra-deformable vesicles. Cevc et al. [22] compared the penetration ability of ultra-deformable vesicles (so called Transfersomes), liposomes, and mixed micelles by CLSM and observed that mixed micelles were restricted to the top-most part of stratum corneum whereas Transfersomes penetrated to a deeper skin layer. As a result of high elasticity and low surfactant concentrations, C16-, CS16- and T16-vesicles were chosen as lead formulations for BLM-vesicles.

Preparations of C16-BLM exhibited significantly higher BLM entrapment efficiency than T16- and EPC-BLM vesicles (Table 3). That may be due to electrostatic interaction between negatively-charged Cholate and positively-charged BLM, but also interaction between BLM and Sit-G molecules incorporated into the membrane. It might be one of the reasons why CS16-vesicles obtained a high entrapment efficiency of 28% despite being less negatively-charged than C16-vesicles.

Following topical application onto rats, CS16-BLM delivered significantly higher concentrations of BLM into the skin compared to C16-BLM, EPC-BLM and BLM solutions 3 h after application. Moreover, most of the BLM that had been absorbed was then distributed quickly into the epidermis and dermis. Vesicles enhanced BLM penetration and this may be due to EPC temporarily changing the ultrastructual properties of the skin [23,24]. Furthermore, penetration may be augmented by the deformability of vesicles and the presence of Sit-G.

The superior penetration potential of CS16-vesicles was further confirmed by skin penetration studies performed by CLSM analysis with fluorescent probes of DiI and calcein. CLSM images taken of rat skin after 3 h incubation with fluorescent probes showed that calcein did not penetrate into the skin when applied as a solution, but was transported into the bottom of SC layer when encapsulated in CS16-vesicles. This finding suggests that ultra-deformable vesicles can deliver hydrophilic drugs encapsulated in vesicles.

CS-BLM increased significantly penetration of BLM into viable epidermis and dermis than C-BLM, suggesting that incorporation of Sit-G into vesicles has a strong penetration enhancing effect. This additional effect of the Sit-G incorporated in a vesicle as absorption enhancer could be attributed to its interactions with the SC lipids. Sit-G may have been incorporated into the SC bilayers, thereby increasing the space of polar domains of these bilayers.

The physicochemical background of Sit-G and Cholate has to be taken into consideration. Sit-G is slightly water-soluble and Cholate is soluble. Cholate 0.16% (w/w) aqueous solution may form mixed micelles despite the CMC of Cholate being observed at 6.2 mM, 0.25% (w/w) [25,26]. Ultra-deformable formulations of BLM may compose of various vesicles, such as liposomes and micelles. Under the conditions used in this study, the effect of micelles on permeation of BLM should not be neglected. However, the ratio of liposome to micelles in CS-BLM has not been estimated at the present time. Further studies will therefore be necessary to investigate the effect of various types of vesicles on skin-permeation enhancer properties.

5. Conclusions

Ultra-deformable formulations containing Sit-G increased entrapment efficiency of BLM and maintained in vitro stability and flexibility. Ultra-deformable vesicles incorporating Sit-G and entrapped with BLM, when applied non-occlusively onto rat skin, significantly increased distribution of BLM in epidermis and dermis compared with ultra-deformable vesicles without Sit-G.

Acknowledgements

We greatly acknowledge Dr. Kent G. Lau for his review of the manuscript. This project was supported in part by a grant from The Promotion and Mutual Aid Corporation for Private Schools of Japan, and by a Grant-in-aid for Scientific Research from the Ministry of Education, Culture, Sports, Science, and Technology of Japan.

References

[1] B.W. Barry, S.L. Bennett, Effect of penetration enhancers on the permeation of mannitol, hydrocortisone and progesterone through human skin, J. Pharm. Pharmacol. 39 (1987) 535–546.
[2] K. Tojo, C.C. Chiang, Y.W. Chien, Drug permeation across the skin: effect of penetrant hydrophilicity, J. Pharm. Sci. 76 (1987) 123–126.
[3] A. Sharma, U.S. Sharma, Liposomes in drug delivery: progress and limitations, Int. J. Pharm. 154 (1997) 123–140.
[4] G. Cevc, A. Schatzlein, D. Gebauer, G. Blume, Ultrahighefficiency of drug and peptide transfer through intact skin by means of novel drug carriers, transfersomes, in: K.R. Bain, J. Hadgkraft, W.J. James, K.A. Water (Eds.), Prediction of Percutaneous Penetration, vol. 3b, STS Publishing, Cardiff, 1993, pp. 226–236.
[5] G. Cevc, G. Blume, Lipid vesicles penetrate into intact skin owing to the transdermal osmotic gradients and hydration force, Biochim. Biophys. Acta 1104 (1992) 226–232.
[6] M.E. Planas, P. Gonzalez, L. Rodriguez, S. Sanchez, G. Cevc, Noninvasive percutaneous induction of topical analgesia by a new type of drug carrier, and prolongation of local pain insensitivity by anesthetic liposomes, Anesth. Analg. 75 (1992) 615–621.
[7] G. Cevc, G. Blume, Biological activity and characteristics of triamcinolone-acetonide formulated with the self-regulating drug carriers, transfersomes, Biochim. Biophys. Acta 1614 (2003) 156–164.
[8] G.M. El Maghraby, A.C. Williams, B.W. Barry, Oestradiol skin delivery from ultradeformable liposomes: refinement of surfactant concentration, Int. J. Pharm. 196 (2000) 63–74.
[9] K.G. Lau, S. Chopra, Y. Maitani, Entrapment of bleomycin in ultra-deformable liposomes, S.T.P. Pharma Sci. 13 (2003) 237–239.
[10] K.G. Lau, Y. Hattori, S. Chopra, E.A. O'Toole, A. Storey, T. Nagai, Y. Maitani, Ultra-deformable liposomes containing bleomycin: in vitro stability and toxicity on human cutaneous keratinocyte cell lines, Int. J. Pharm. 300 (2005) 4–12.
[11] K. Muramatsu, Y. Maitani, K. Takayama, T. Nagai, The relationship between the rigidity of the liposomal membrane and the absorption of insulin after nasal administration of liposomes modified with an enhancer containing insulin in rabbits, Drug Dev. Ind. Pharm. 25 (1999) 1099–1105.
[12] K. Nakamura, K. Takayama, T. Nagai, Y. Maitani, Regional intestinal absorption of FITC-dextran 4400 with nanoparticles based on beta-sitosterol beta-D-glucoside in rats, J. Pharm. Sci. 92 (2003) 311–318.
[13] G. Cevc, A. Schatzlein, G. Blume, Transdermal drug carriers: basic properties, optimization and transfer efficiency in the case of epicutaneously applied peptides, J. Control. Release 36 (1995) 3–16.
[14] G. Cevc, D. Gebauer, J. Stieber, A. Schatzlein, G. Blume, Ultraflexible vesicles, transfersomes, have an extremely low pore penetration resistance

and transport therapeutic amounts of insulin across the intact mammalian skin, Biochim. Biophys. Acta 1368 (1998) 201–215.
[15] W.R. Perkins, S.R. Minchey, P.L. Ahl, A.S. Janoff, The determination of liposome captured volume, Chem. Phys. Lipids 64 (1993) 197–217.
[16] H.P. Fiedler, J. Wachter, High-performance liquid chromatographic determination of bleomycins, J. Chromatogr. 536 (1991) 343–347.
[17] A.D. Bangham, M.M. Standish, J.C. Watkins, Diffusion of univalent ions across the lamellae of swollen phospholipids, J. Mol. Biol. 13 (1965) 238–252.
[18] A.D. Bangham, Membrane models with phospholipids, Prog. Biophys. Mol. Biol. 18 (1968) 29–95.
[19] B.A. van den Bergh, P.W. Wertz, H.E. Junginger, J.A. Bouwstra, Elasticity of vesicles assessed by electron spin resonance, electron microscopy and extrusion measurements, Int. J. Pharm. 217 (2001) 13–24.
[20] L.J. Korstanje, G. van Ginkel, Y.K. Levine, Effects of steroid molecules on the dynamical structure of dioleoylphosphatidylcholine and digalactosyldiacylglycerol bilayers, Biochim. Biophys. Acta 1022 (1990) 155–162.
[21] C. Hofer, R. Hartung, R. Gobel, P. Deering, A. Lehmer, J. Breul, New ultradeformable drug carriers for potential transdermal application of interleukin-2 and interferon-alpha: theoretic and practical aspects, World J. Surg. 24 (2000) 1187–1189.
[22] G. Cevc, G. Blume, A. Schatzlein, D. Gebauer, A. Paul, The skin: a pathway for systemic treatment with patches and lipid-based agent carriers, Adv. Drug Deliv. Rev. 18 (1996) 349–378.
[23] A. Blume, M. Jansen, M. Ghyczy, J. Gareiss, Interaction of phospholipid liposomes with lipid model mixtures for stratum corneum lipids, Int. J. Pharm. 99 (1993) 219–228.
[24] H.E. Hofland, J.A. Bouwstra, H.E. Bodde, F. Spies, H.E. Junginger, Interactions between liposomes and human stratum corneum in vitro: freeze fracture electron microscopical visualization and small angle X-ray scattering studies, Br. J. Dermatol. 132 (1995) 853–866.
[25] R. Ninomiya, K. Matsuoka, Y. Moroi, Micelle formation of sodium chenodeoxycholate and solubilization into the micelles: comparison with other unconjugated bile salts, Biochim. Biophys. Acta 1634 (2003) 116–125.
[26] H. Sugioka, K. Matsuoka, Y. Moroi, Temperature effect on formation of sodium cholate micelles, J. Colloid Interface Sci. 259 (2003) 156–162.

Available online at www.sciencedirect.com
SCIENCE DIRECT®
Journal of Controlled Release 112 (2006) 329–332
journal of controlled release
www.elsevier.com/locate/jconrel

Enhanced antitumor effect of camptothecin loaded in long-circulating polymeric micelles

Kumi Kawano [a], Masato Watanabe [a], Tatsuhiro Yamamoto [b], Masayuki Yokoyama [b], Praneet Opanasopit [c], Teruo Okano [c], Yoshie Maitani [a,*]

[a] *Institute of Medicinal Chemistry, Hoshi University, 2-4-41 Ebara, Shinagawa-ku, Tokyo 142-8501, Japan*
[b] *Kanagawa Academy of Science and Technology, KSP East 404, Sakado 3-2-1, Takatsu-ku, Kawasaki-shi, Kanagawa 213-0012, Japan*
[c] *Institute of Advanced Biomedical Engineering and Science, Tokyo Women's Medical University, Kawada-cho 8-1, Shinjuku-ku, Tokyo 162-8666, Japan*

Received 18 October 2005; accepted 20 March 2006
Available online 27 March 2006

Abstract

A water-insoluble antitumor agent, camptothecin (CPT) was successfully incorporated into polymeric micelles formed from poly(ethylene glycol)-poly(benzyl aspartate) block copolymers (CPT-loaded polymeric micelles). Antitumor effects and biodistribution of CPT-loaded micelles were evaluated in mice subcutaneously transplanted by colon 26 tumor cells. Tumor growth was significantly inhibited after a single i.v. injection of CPT-loaded polymeric micelles at doses of either 15 or 30 mg/kg. Efficacy of a single high-dose injection was comparable to low dose multiple injections. CPT loaded in polymeric micelles showed prolonged blood circulation and higher accumulation in tumors compared with CPT in solution. Polymeric micelle systems offer a stable and effective platform for cancer chemotherapy with CPT.

Keywords: Camptothecin; Polymeric micelle; Antitumor effect; Biodistribution; Colon 26 tumor

1. Introduction

In cancer chemotherapy, the usage of anticancer drugs has been limited by their toxic side-effects in normal organs. Anticancer drug carriers, such as liposomes, microspheres and polymeric systems, have been developed to target and improve their efficacy toward malignant cells, and to reduce toxicity. Long-circulating carriers with nanoscopic dimensions in the bloodstream can passively deliver chemotherapeutic agents to tumor sites via an enhanced permeability and retention effect (EPR effect) [1,2].

Polymeric micelles are prepared from block copolymers possessing both hydrophilic and hydrophobic chains, and they have received much attention in drug delivery research. Their innate characteristics for drug targeting include solubilization of hydrophobic molecules, small particle size, high structural stability, extended drug release, and prevention of rapid clearance by the reticuloendothelial system. Anticancer drug targeting using polymeric micelles was first employed in enhancing the in vivo anticancer activity of doxorubicin [3,4]. Such systems have now been applied to other anticancer drugs, such as paclitaxel [5], cisplatin [6], methotrexate [7] and KRN 5500 [8].

Camptothecin (CPT), a plant alkaloid extracted from *Camptotheca acuminate*, acts as a potent antitumor agent by inhibiting the nuclear enzyme topoisomerase I. CPT inhibits the growth of a wide range of tumors [9,10]. However, the major drawbacks of the drug have always been water insolubility and lactone instability. The lactone ring in CPT plays an important role in the drug's biological activity but it exists in a pH-dependent equilibrium with an open ring carboxylate form (Fig. 1(A)). The lactone ring opens at physiological pH or above, making this drug much less active and highly toxic (such as myelosuppression, haemorrhagic cystitis and diarrhea), and precludes its clinical use.

In our previous study, CPT was successfully incorporated in poly(ethylene glycol)-poly(L-aspartate ester) block copolymer micelles with high incorporation efficiency by optimizing its preparation method and copolymer structure [11,12]. Polymers exhibiting 60–70% benzyl esterification of the aspartate chain yielded micelles that were stable in blood plasma [13]. In this report, the antitumor effects and biodistribution of CPT-loaded polymeric micelles were evaluated in mice bearing colon

* Corresponding author. Tel./fax: +81 3 5498 5048.
E-mail address: yoshie@hoshi.ac.jp (Y. Maitani).

0168-3659/$ - see front matter © 2006 Elsevier B.V. All rights reserved.
doi:10.1016/j.jconrel.2006.03.012

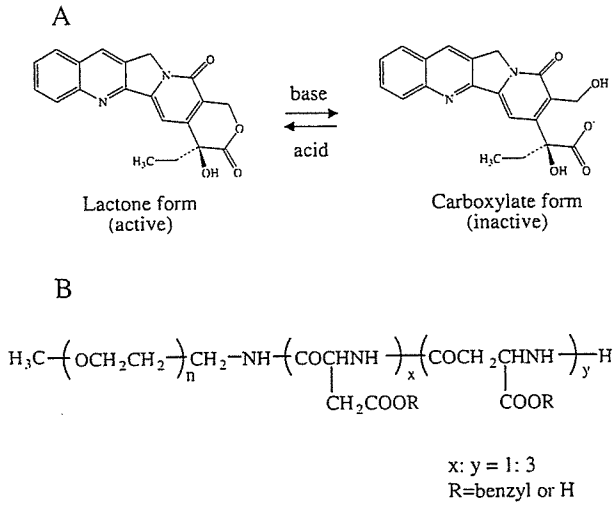

Fig. 1. pH-dependent equilibrium of camptothecin (A) and chemical structure of block copolymer (PEG-P(Asp(Bz-70))) (B).

26 solid tumors. Polymeric micelles loaded with CPT prolonged its blood circulation time and enhanced its antitumor effect due to tumor accumulation by the EPR effect.

2. Materials and methods

2.1. Preparation of CPT-loaded polymeric micelles

Poly(ethylene glycol)-poly(benzyl aspartate-70) block copolymer (PEG-P(Asp(Bz-70))) was synthesized by benzylesterification of poly(ethylene glycol)-poly(aspartic acid) as described previously [11]. PEG-P(Asp(Bz-70)) was composed of the poly(ethylene glycol) (PEG) block of molecular weight of 5000 determined by gel-permeation chromatography, and the p(Asp) block possessing 25 units of the aspartic acid residues on average determined by ^{1}H NMR spectroscopy. Seventy percent of the aspartic acid residue was esterified with benzyl group determined by ^{1}H NMR spectroscopy (Fig. 1(B)). From these three values, the molecular weight of PEG-P(Asp(Bz-70)) was calculated to be 9700. (s)-(+)-Camptothecin (CPT, Aldrich Chem. Co.) was incorporated into polymeric micelles by an evaporation method as reported previously [12], using 2 mg of CPT and 5 mg of PEG-P(Asp(Bz-70)). CPT incorporation efficiency in micelle to the drug in preparation was 63%. The average particle size was 191.8±12.7 nm, measured by dynamic light scattering particle size analyzer (ELS-800, Otsuka Electronics, Osaka, Japan).

2.2. Antitumor activity

Antitumor activity of CPT-loaded polymeric micelles was evaluated with mouse bearing colon adenocarcinoma 26. The animal experiments were conducted in accordance with the Guiding Principles for the Care and Use of Laboratory Animals of Hoshi University. Colon 26 cells (1×10^4 cells/0.1 ml) were transplanted into CDF_1 female mice (5 weeks old, Sankyo Labo Service Corporation, Tokyo, Japan) subcutaneously, and drug injection was started when tumor volume reached approximately 100 mm^3. Drug was injected into a tail vein once or three times at a three day interval. CPT solution was prepared by dissolving CPT (13 mg) in 50 ml of polyethylene glycol 400, propylene glycol and polysorbate 80 (40:50:2, volume ratio) [14]. Tumor volume and body weight were measured for individual animals. Tumor volume was calculated as follows; volume$=\pi/6\times LW^2$, where L is the long diameter and W is the short diameter. Percentage of tumor growth inhibition (T/C%) was calculated from relative tumor volume at day 8, following the equation: T/C%$=100\times$(mean relative tumor volume of treated group)/(mean relative tumor volume of control group).

2.3. CPT biodistribution in tumor bearing mice

CPT biodistribution was evaluated in CDF_1 female mice (5 weeks old) subcutaneously transplanted by colon 26 cells (1×10^4 cells/0.1 ml) after tumor volume reached approximately 100 mm^3. CPT-loaded micelles and CPT solution were intravenously administered via lateral tail veins at a dose of 2.5 mg/kg. Twenty-four hours after injection, blood was collected with heparinized syringe and centrifuged to obtain the plasma. The tumor and major tissues were excised and homogenized in phosphate buffered saline (pH 7.4). For the determination of CPT, an aliquot of plasma or the tissue homogenate was acidified with the aqueous phosphoric acid (0.15 M) and then CPT was extracted with chloroform:methanol (4:1 volume ratio). After centrifugation of the mixture, 25 μl of the chloroform:methanol layer was directly analyzed by the HPLC system (Shimadzu Corp., Japan), using a Tosoh TSK-gel ODS-80Ts column (150×4.6 mm I.D., Tosoh Corp., Japan) and a fluorescence detector (excitation: 369 nm, emission: 426 nm). The mobile phase was composed of 23:77 (v/v) acetonitrile-triethylamine acetate buffer (1% (v/v) adjusted to pH 5.5 with glacial acetic acid) at a flow rate 1.0 ml/min [15]. Standard curve with concentrations ranging from 25 ng/ml to 1.0 μg/ml of the drug exhibited good linearity with a correlation coefficient of 0.999.

3. Results and discussion

3.1. Antitumor effect of CPT-loaded polymeric micelles in colon 26 solid tumors

Antitumor effect of CPT-loaded polymeric micelles was evaluated in mice bearing colon 26 solid tumors (Fig. 2). In a preliminary study, murine weight loss was over 20% (three days after injection) and it took two days to recover from a single i.v. administration of 40 mg/kg CPT-loaded polymeric micelles to normal CDF_1 mouse (data not shown). This result suggested that 30 mg/kg would be the maximum dose for murine cancer treatment. The dose of CPT solution (15 mg/kg) was decided by its solubility (0.26 mg/ml) in the solvent used and tolerable body weight loss for treatment. Treatment with CPT solution showed tumor growth inhibition (T/C%) of 49.6% at day 8, whereas polymeric micelles treated at either 15 or 30 mg/kg of CPT were 27.5% and 18.5%, respectively (Fig. 2(A)). Furthermore, these polymeric preparations significantly inhibited tumor growth at

day 8 compared with control ($P<0.01$) without significant adverse effects, such as weight loss ($P>0.05$) (Fig. 2(B)).

When the total CPT dose was fixed at 30 mg/kg, a single i.v. injection of CPT-loaded polymeric micelles exhibited comparable inhibition of tumor growth to a triple injection at a dose of 10 mg/kg/day (T/C% of 42.1%) (Fig. 2 (C)). Cytotoxicity of CPT and other topoisomerase I inhibitors is S-phase specific and in vivo studies have suggested that multiple administration of CPT-derivatives were effective against tumors [16]. CPT conjugated with poly(L-glutamic acid) (PG-CPT) or *N*-(2-hydroxypropyl) methacrylamide (HPMA-CPT) needed frequent administration in order to be effective, even though enhanced accumulation was observed in the tumor [17–19]. Furthermore, at equivalent drug levels, repeated administration (40 mg/kg × 4, 4 day interval) of PG-CPT was more efficacious than a single bolus (160 mg/kg) [17]. This discrepancy may be due to a difference in the rate of release of free CPT from the polymeric carriers. Although CPT has been shown to release slowly from PG-CPT and HPMA-CPT [17,19], CPT-loaded polymeric micelles quickly shed nearly half of its load within 24 h, despite retardation by highly benzyl esterified polymer [12]. These findings suggest that the rapid bioavailability of free CPT from the polymeric micelles, relative to other polymeric carriers, may indeed improve antitumor activity subsequent to the passive accumulation of polymeric carriers in the tumor tissue.

3.2. Tumor accumulation of CPT-loaded polymeric micelles

The biodistribution profiles of CPT-loaded polymeric micelles and CPT solution were determined 24 h after i.v. injection of 2.5 mg/kg into mice bearing colon 26 tumor (Fig. 3). Blood

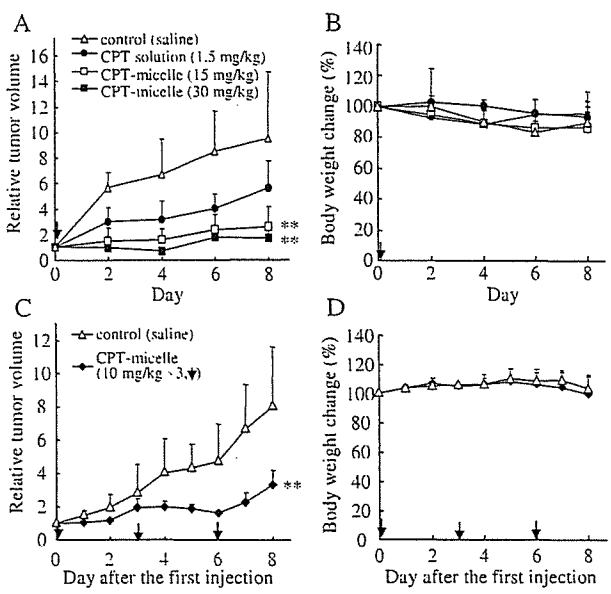

Fig. 2. Antitumor activity (A, C) and body weight change (B, D) after a single (A, B) and a triple (C, D) injection of CPT-loaded polymeric micelles in mice bearing colon 26 tumor. Arrows indicate the day of drug injections. Tumor volumes are plotted in ratios to the initial volume at day 0. Each value represents the mean ± S.D. ($n=4$–5). **: $P<0.01$, compared with control at day 8 (Scheffe's *F*-test).

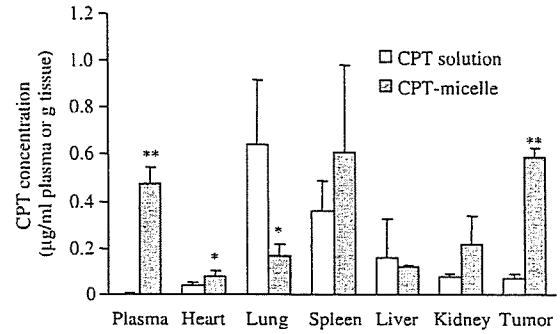

Fig. 3. CPT biodistribution in mice bearing colon 26 tumor 24 h after i.v. injection of CPT-loaded polymeric micelles and CPT solution at a dose of 2.5 mg/kg. Each value represents the mean ± S.D. ($n=3$). *: $P<0.05$, **: $P<0.01$, compared with CPT solution (Students' *t*-test).

plasma levels of CPT-loaded micelles (1.1% of injected dose) were approximately 150 times higher than CPT solution. Tumor accumulation of CPT-loaded polymeric micelles (approximately 1.3% of injected dose per g tissue) was nearly 8 times higher than CPT solution. Elevated pulmonary CPT levels by CPT solution may be due to embolization of lung capillaries arising from drug precipitation [14].

The pharmacokinetic (area under the plasma concentration–time curve, AUC) profile of CPT-loaded polymeric micelles was approximately 17 times higher than CPT solution when administered at a dose of 2.5 mg/kg in ddY mice [13]. Drug carriers with a prolonged circulation time are able to increase their accumulation in tumor tissues by the EPR effect and, consequently, improve antitumor activity. Furthermore, polymeric micelles could maintain CPT lactone form even in the presence of serum [12]. These characteristics suggest that polymeric micelles possess the ability to deliver large amounts of CPT, in its most active lactone form, to the tumor site by passive targeting with a long-circulating carrier.

4. Conclusion

Polymeric micelles increased the antitumor effects of camptothecin (CPT) in mice subcutaneously transplanted with a colon 26 tumor. The observed therapeutic efficacy of micelles is probably related to the extended circulation time. Passive accumulation of this preparation in tumor sites induced a similar level of significant tumor regression, whether from a single bolus of 30 mg/kg CPT or three repeated doses of 10 mg/kg. Polymeric micelle systems offer a stable and effective platform for cancer chemotherapy with camptothecin.

References

[1] Y. Matsumura, H. Maeda, A new concept for macromolecular therapeutics in cancer chemotherapy: mechanism of tumoritropic accumulation of proteins and the antitumor agent smancs, Cancer Res. 46 (1986) 6387–6392.
[2] H. Maeda, The enhanced permeability and retention (EPR) effect in tumor vasculature. The key role of tumor-selective macromolecular drug targeting, Adv. Enzyme Regul. 41 (2000) 189–207.
[3] M. Yokoyama, T. Okano, Y. Sakurai, H. Ekimoto, C. Shibazaki, K. Kataoka, Toxicity and antitumor activity against solid tumors of

micelle-forming polymeric anticancer drug and its extremely long circulation in blood, Cancer Res. 51 (1991) 3229–3236.
[4] M. Yokoyama, S. Fukushima, R. Uehara, K. Okamoto, K. Kataoka, Y. Sakurai, T. Okano, Characterization of physical entrapment and chemical conjugation of adriamycin in polymeric micelles and their design for in vivo delivery to a solid tumor, J. Control. Release 50 (1998) 79–92.
[5] T.Y. Kim, D.W. Kim, J.Y. Chung, S.G. Shin, S.C. Kim, D.S. Heo, N.K. Kim, Y.J. Bang, Phase I and pharmacokinetic study of Genexol-PM, a cremophor-free, polymeric micelle-formulated paclitaxel, in patients with advanced malignancies, Clin. Cancer Res. 10 (2004) 3708–3716.
[6] N. Nishiyama, S. Okazaki, H. Cabral, M. Miyamoto, Y. Kato, Y. Sugiyama, K. Nishio, Y. Matsumura, K. Kataoka, Novel cisplatin-incorporated polymeric micelles can eradicate solid tumors in mice, Cancer Res. 63 (2003) 8977–8983.
[7] Y. Li, G.S. Kwon, Methotrexate esters of poly(ethylene oxide)-block-poly (2-hydroxyethyl-L-aspartamide). Part I: Effects of the level of methotrexate conjugation on the stability of micelles and on drug release, Pharm. Res. 17 (2000) 607–611.
[8] M. Yokoyama, A. Satoh, Y. Sakurai, T. Okano, Y. Matsumura, T. Kakizoe, K. Kataoka, Incorporation of water-insoluble anticancer drug into polymeric micelles and control of their particle size, J. Control. Release 55 (1998) 219–229.
[9] B.C. Giovanella, H.R. Hinz, A.J. Kozielski, J.S. Stehlin Jr., R. Silber, M. Potmesil, Complete growth inhibition of human cancer xenografts in nude mice by treatment with 20-(S)-camptothecin, Cancer Res. 51 (1991) 3052–3055.
[10] B.C. Giovanella, J.S. Stehlin, M.E. Wall, M.C. Wani, A.W. Nicholas, L.F. Liu, R. Silber, M. Potmesil, DNA topoisomerase I-targeted chemotherapy of human colon cancer in xenografts, Science 246 (1989) 1046–1048.
[11] M. Yokoyama, P. Opanasopit, T. Okano, K. Kawano, Y. Maitani, Polymer design and incorporation methods for polymeric micelle carrier system containing water-insoluble anti-cancer agent camptothecin, J. Drug Target. (2004) 373–384.
[12] P. Opanasopit, M. Yokoyama, M. Watanabe, K. Kawano, Y. Maitani, T. Okano, Block copolymer design for camptothecin incorporation into polymeric micelles for passive tumor targeting, Pharm. Res. 21 (2004) 2001–2008.
[13] M. Watanabe, K. Kawano, M. Yokoyama, P. Opanasopit, T. Okano, Y. Maitani, Preparation of camptothecin-loaded polymeric micelles and evaluation of their incorporation and circulation stability, Int. J. Pharm. 308 (2006) 183–189.
[14] S.C. Yang, L.F. Lu, Y. Cai, J.B. Zhu, B.W. Liang, C.Z. Yang, Body distribution in mice of intravenously injected camptothecin solid lipid nanoparticles and targeting effect on brain, J. Control. Release 59 (1999) 299–307.
[15] D.L. Warner, T.G. Burke, Simple and versatile high-performance liquid chromatographic method for the simultaneous quantitation of the lactone and carboxylate forms of camptothecin anticancer drugs, J. Chromatogr., B, Biomed. Sci. Appl. 691 (1997) 161–171.
[16] J. O'Leary, F.M. Muggia, Camptothecins: a review of their development and schedules of administration, Eur. J. Cancer 34 (1998) 1500–1508.
[17] Y. Zou, Q.P. Wu, W. Tansey, D. Chow, M.C. Hung, C. Charnsangavej, S. Wallace, C. Li, Effectiveness of water soluble poly(L-glutamic acid)-camptothecin conjugate against resistant human lung cancer xenografted in nude mice, Int. J. Oncol. 18 (2001) 331–336.
[18] V.R. Caiolfa, M. Zamai, A. Fiorino, E. Frigerio, C. Pellizzoni, R. d'Argy, A. Ghiglieri, M.G. Castelli, M. Farao, E. Pesenti, M. Gigli, F. Angelucci, A. Suarato, Polymer-bound camptothecin: initial biodistribution and antitumour activity studies, J. Control. Release 65 (2000) 105–119.
[19] M. Zamai, M. VandeVen, M. Farao, E. Gratton, A. Ghiglieri, M.G. Castelli, E. Fontana, R. D'Argy, A. Fiorino, E. Pesenti, A. Suarato, V.R. Caiolfa, Camptothecin poly[*n*-(2-hydroxypropyl) methacrylamide] copolymers in antitopoisomerase-I tumor therapy: intratumor release and antitumor efficacy, Mol. Cancer Ther. 2 (2003) 29–40.

Available online at www.sciencedirect.com
SCIENCE DIRECT
ELSEVIER
Colloids and Surfaces A: Physicochem. Eng. Aspects 284–285 (2006) 276–283
COLLOIDS AND SURFACES A
www.elsevier.com/locate/colsurfa

The structure of artificial lipids possessing oligo(ethylene glycol) and their behavior in water

Taichi Yoshitomi [a,b], Sawataka Yabuki [a,b], Hiroko Kawakami [a,c], Reiko Sato [a,c], Kazunori Toma [a,c,*], Masahiko Furuhata [d], Yoshie Maitani [d]

[a] *The Noguchi Institute, 1-8-1, Kaga, Itabashi, Tokyo 173-0003, Japan*
[b] *Department of Industrial Chemistry, Faculty of Engineering, Tokai University, 1117, Kitakaname, Hiratuka, Kanagawa 259-1292, Japan*
[c] *CREST, Japan Science and Technology Agency, 4-1-8, Honcho, Kawaguchi, Saitama 332-0012, Japan*
[d] *Institute of Medicinal Chemistry, Hoshi University, 2-4-41, Ebara, Shinagawa, Tokyo 142-8501, Japan*

Received 24 June 2005; received in revised form 24 February 2006; accepted 24 February 2006
Available online 5 April 2006

Abstract

The synthesis of artificial lipids containing 3,5-bis- or 3,4,5-tris(dodecyloxy)benzamide and oligo(ethylene glycol) (OEG) moieties is described. The terminal group was either an alcohol or an amine, and the length of ethylene glycol unit was three, six, eight or nine. The critical micelle concentration (CMC) of these artificial lipids was determined by a fluorescent probe method using Nile red. The CMC values were lower than that of single chain OEG alkyl ether surfactants. The 3,4,5-tris(dodecyloxy)benzamide derivatives had a higher CMC ($\sim 10^{-5}$ M) than the 3,5-bis(dodecyloxy)benzamide derivatives ($\sim 10^{-6}$ M). The particle size distribution of aqueous dispersions of the artificial lipids was determined using a dynamic light scattering method. The particle size distributions were different depending on the length of OEG chain, the number of hydrophobic chains, and the terminal functional group. Short OEG derivatives formed insoluble aggregates even at low concentrations, and a long OEG derivative produced large water soluble aggregates.

Keywords: Artificial lipids; Critical micelle concentration; Particle size distribution

1. Introduction

We are in the process of studying biological applications of functional molecules, such as carbohydrates and peptides, by connecting them to artificial lipid moieties of 3,5-bis- or 3,4,5-tris(dodecyloxy)benzamide, or related compounds [1,2]. Such conjugate molecules can be immobilized on hydrophobic surfaces using the lipid portion as a handle, permitting functional molecules to be present on the surface. In previous studies, we have shown carbohydrate specific binding of lectins [2], the stimulating effect of galactose on rat hepatocytes [3,4], the expansion effect of galactose-6-sulfate on human blood progenitor cells [5], and the effect of cell adhesion peptides on interferon-β production in NB1-RGB cells [6].

For some applications, however, nonspecific interactions due to the lipid portion or the hydrophobic surface become problematic. In an attempt to minimize such nonspecific hydrophobic interactions, we introduced oligo(ethylene glycol) (OEG) moieties to our artificial lipids, and found that such compounds could be dispersed in water. Although single chain alkyl ethers of OEG are well-characterized nonionic surfactants [7–9], studies in which OEG ethers with two or more hydrophobic alkyl chains are used are rare. Therefore, we synthesized several derivatives of artificial lipids composed of OEG and 3,5-bis- or 3,4,5-tris(dodecyloxy)benzamide moieties, and examined their behavior in water by determining their critical micelle concentration (CMC) and particle size distribution.

2. Materials and methods

2.1. General

All reagents and anhydrous solvents were purchased from commercial suppliers and were used as provided. ^{1}H NMR

* Corresponding author. Tel.: +81 3 5944 3216; fax: +81 3 5944 3216.
E-mail address: toma@noguchi.or.jp (K. Toma).

0927-7757/$ – see front matter © 2006 Elsevier B.V. All rights reserved.
doi:10.1016/j.colsurfa.2006.02.057

spectra were determined on either a JNMEX-400 or an ECA-600 spectrometer (JEOL, Tokyo, Japan). Electrospray ionization mass spectrometry (ESIMS) was carried out on a Mariner biospectrometry workstation (Applied Biosystems Japan, Tokyo, Japan).

2.1.1. N-(8-Amino-3,6-dioxaoctyl)-3,5-bis(dodecyloxy)-benzamide (1)

3,5-Bis(dodecyloxy)benzoic acid [1] (500 mg, 1.02 mmol), 1-hydroxybenzotriazole hydrate (170 mg, 1.22 mmol), and water soluble carbodiimide HCl (230 mg, 1.22 mmol) were dissolved in CH_2Cl_2 (10 ml). The mixture was stirred at room temperature for 1 h, and added dropwise to a CH_2Cl_2 (10 ml) solution of 3,6-dioxa-1,8-octanediamine (0.24 ml, 2.04 mmol). The reaction was allowed to proceed at room temperature for 1 h, and then terminated by adding saturated aqueous $NaHCO_3$. The organic layer was separated, and the water layer was extracted with CH_2Cl_2. The combined organic layer was washed with saturated NaCl aq, dried over Na_2SO_4 and concentrated in vacuo. The crude product was purified by silica gel column chromatography using $CHCl_3$–MeOH (9:1) as the eluent to give **1** (250 mg, 39%). ^{1}H NMR ($CDCl_3$, 400 MHz), δ 6.96 (d, 2H, J = 2.0 Hz, aromatic H), 6.88 (s, 1H, –CONH), 6.54 (t, 1H, J = 2.1 Hz, aromatic H), 3.96 (t, 4H, J = 6.5 Hz, ArO–CH_2), 3.62 (m, 10H, O–$(CH_2)_2$–O), 3.02 (t, 2H, J = 5.0 Hz, N–CH_2), 1.74 (m, 4H, ArOC–CH_2), 1.42 (m, 4H, $ArOC_2$–CH_2) 1.26 (m, 32H, $ArOC_3$–C_8H_{16}), 0.88 (6H, t, J = 7.2 Hz, –CH_3). ESIMS, found: m/z 621.43, calcd. for $C_{37}H_{69}N_2O_5$ ($[M+H]^+$): 621.52.

2.1.2. N-(17-Amino-3,6,9,12,15-pentaoxaheptadecyl)-3,5-bis(dodecyloxy)benzamide (2)

Similar to **1**, **2** (330 mg, 37%) was synthesized from 3,5-bis(dodecyloxy)benzoic acid (580 mg, 1.19 mmol) and 3,6,9,12,15-pentaoxa-1,17-heptadecanediamine (0.24 ml, 2.04 mmol). ^{1}H NMR ($CDCl_3$, 400MHz), δ 7.01 (s, 1H, –CONH), 6.91 (d, 2H, J = 2.1 Hz, aromatic H), 6.54 (t, 1H, J = 2.4 Hz, aromatic H), 3.96 (t, 4H, J = 6.5 Hz, ArO–CH_2), 3.61 (m, 20H, O–$(CH_2)_2$–O), 3.56 (t, 2H, J = 5.5 Hz, O–CH_2–C–N), 3.09 (t, 2H, J = 5.2 Hz, N–CH_2), 1.77 (m, 4H, ArOC–CH_2), 1.48 (m, 4H, $ArOC_2$–CH_2), 1.34 (m, 32 H, $ArOC_3$–C_8H_{16}), 0.89 (t, 6H, J = 7.2 Hz, –CH_3). ESIMS, found: m/z 753.59, calcd. for $C_{43}H_{81}N_2O_8$ ($[M+H]^+$): 753.45.

2.1.3. N-(26-Amino-3,6,9,12,15,18,21,24-octaoxahexaicosyl)-3,5-bis(dodecyloxy)benzamide (3)

Similar to **1**, **3** (293 mg, 50%) was synthesized from 3,5-bis(dodecyloxy)benzoic acid (324 mg, 0.66 mmol) and 3,6,9,12,15,18,21,24-octaoxa-1,26-hexaicosanediamine (545 mg, 1.32 mmol). ^{1}H NMR ($CDCl_3$, 400 MHz), δ 7.08 (s, 1H, –CONH), 6.91 (d, 2H, J = 2.1 Hz, aromatic H), 6.54 (t, 1H, J = 2.4 Hz, aromatic H), 3.96 (t, 4H, J = 6.5 Hz, ArO–CH_2), 3.63 (m, 32H, O–$(CH_2)_2$–O), 3.53 (t, 2H, J = 5.2 Hz, O–CH_2–C–N), 2.88 (t, 2H, J = 5.5 Hz, N–CH_2), 1.76 (m, 4H, ArOC–CH_2), 1.42 (m, 4H, $ArOC_2$–CH_2), 1.30 (m, 32 H, $ArOC_3$–C_8H_{16}), 0.88 (t, 6H, J = 6.9 Hz, –CH_3). ESIMS found: m/z 885.67, calcd. for $C_{49}H_{93}N_2O_{11}$ ($[M+H]^+$): 885.66.

2.1.4. N-(8-Amino-3,6-dioxaoctyl)-3,4,5-tris(dodecyloxy)benzamide (4)

Similar to **1**, **4** (1.12 g, 69%) was synthesized from 3,4,5-tris(dodecyloxy)benzoic acid [1] (1.10 g, 1.63 mmol) and 3,6-dioxa-1,8-octanediamine (1.21 g, 8.14 mmol). ^{1}H NMR ($CDCl_3$, 400 MHz), δ 6.99 (s, 2H, aromatic H), 6.72 (s, 1H, –CONH), 4.00 (t, 6H, J = 5.2 Hz, ArO–CH_2), 3.65 (8H, m, O–$(CH_2)_2$–O), 3.50 (t, 2H, J = 5.2 Hz, O–CH_2–C–N), 2.83 (t, 2H, J = 5.2 Hz, N–CH_2), 1.76 (m, 6H, ArOC–CH_2), 1.26 (m, 54H, $ArOC_2$–C_9H_{18}), 0.88 (t, 9H, J = 6.8 Hz, –CH_3). ESIMS, found: m/z 805.63, calcd. for $C_{49}H_{93}N_2O_6$ ($[M+H]^+$): 805.67.

2.1.5. N-(17-Amino-3,6,9,12,15-pentaoxaheptadecyl)-3,4,5-tris(dodecyloxy)benzamide (5)

Similar to **1**, **5** (1.42 g, 53%) was synthesized from 3,4,5-tris(dodecyloxy)benzoic acid (1.94 g, 2.87 mmol) and 3,6,9,12,15-pentaoxa-1,17-heptadecanediamine (2.42 g, 8.63 mmol). ^{1}H NMR ($CDCl_3$, 400 MHz), δ 7.01 (s, 2H, aromatic H), 6.93 (s, 1H, –CONH), 4.00 (t, 6H, J = 6.2 Hz, $ArOCH_2$), 3.63 (20H, m, O–$(CH_2)_2$–O), 3.48 (t, 2H, J = 5.2 Hz, O–CH_2–C–N), 2.84 (t, 2H, J = 5.2 Hz, N–CH_2), 1.77 (m, 6H, ArOC–CH_2), 1.26 (m, 54H, $ArOC_2$–C_9H_{18}), 0.88 (t, 9H, J = 6.8 Hz, –CH_3). ESIMS, found: m/z 937.57, calcd. for $C_{55}H_{105}N_2O_9$ ($[M+H]^+$): 937.78.

2.1.6. N-(23-Amino-3,6,9,12,15,18,21-heptaoxatriicosyl)-3,4,5-tris(dodecyloxy)benzamide (6)

Similar to **1**, **6** (283 mg, 50%) was synthesized from 3,4,5-tris(dodecyloxy)benzoic acid (369 mg, 0.55 mmol) and 3,6,9,12,15,18,21-heptaoxa-1,23-triicosanediamine (498 mg, 1.35 mmol). ^{1}H NMR ($CDCl_3$, 400 MHz), δ 7.15 (s, 1H, –CONH), 7.07 (s, 2H, aromatic H), 4.01 (t, 6H, J = 6.5 Hz, ArO–CH_2), 3.64 (28H, m, O–$(CH_2)_2$–O), 3.55 (t, 2H, J = 5.2 Hz, O–CH_2–C–N), 2.90 (t, 2H, J = 5.2 Hz, N–CH_2), 1.44 (m, 6H, ArOC–CH_2), 1.26 (m, 54H, $ArOC_2$–C_9H_{18}), 0.88 (t, 9H, J = 6.9 Hz, –CH_3). ESIMS, found: m/z 1025.65, calcd. for $C_{59}H_{113}N_2O_{11}$ ($[M+H]^+$): 1025.83

2.1.7. N-(8-Hydroxy-3,6-dioxaoctyl)-3,5-bis(dodecyloxy)benzamide (7)

Similar to **1**, **7** (1.41 g, 89%) was synthesized from 3,5-bis(dodecyloxy)benzoic acid (1.24 g, 2.53 mmol) and 8-amino-3,6-dioxa-1-octanol (450 mg, 3.03 mmol). ^{1}H NMR ($CDCl_3$, 600 MHz), δ 6.91 (d, 2H, J = 2.4 Hz, aromatic H), 6.70 (s, 1H, –CONH), 6.56 (t, 1H, J = 2.2 Hz, aromatic H), 3.96 (t, 4H, J = 6.6 Hz, ArO–CH_2), 3.67 (m, 12H, O–$(CH_2)_2$–O), 2.49 (bs, 1H, –OH), 1.77 (m, 4H, ArOC–CH_2), 1.42 (m, 4H, $ArOC_2$–CH_2), 1.26 (m, 32H, $ArOC_3$–C_8H_{16}), 0.88 (t, 6H, J = 6.8 Hz, –CH_3). ESIMS, found: m/z 644.48, calcd. for $C_{37}H_{67}NO_6Na$ ($[M+Na]^+$): 644.48

2.1.8. N-(17-Hydroxy-3,6,9,12,15-pentaoxaheptadecyl)-3,5-bis(dodecyloxy)benzamide (8)

Similar to **1**, **8** (3.49 g, 80%) was synthesized from 3,5-bis(dodecyloxy)benzoic acid (2.85 g, 5.81 mmol) and 17-amino-3,6,9,12,15-pentaoxa-1-heptadecanol (2.36 g, 6.39 mmol). ^{1}H NMR ($CDCl_3$, 400 MHz), δ 6.94 (s, 1H, –CONH), 6.91 (d, 2H,

J = 2.2 Hz, aromatic H), 6.54 (t, 1H, J = 2.3 Hz, aromatic H), 3.96 (t, 4H, J = 6.5 Hz, ArO–CH_2), 3.64 (m, 24H, O–$(CH_2)_2$–O), 2.96 (bs, 1H, –OH), 1.76 (m, 4H, ArOC–CH_2), 1.42 (m, 4H, $ArOC_2$–CH_2), 1.26 (m, 32H, $ArOC_3$–C_8H_{16}), 0.88 (t, 6H, J = 6.8 Hz, –CH_3). ESIMS, found: m/z 776.48, calcd. for $C_{43}H_{79}NO_9Na$ ($[M+Na]^+$): 776.56.

2.1.9. N-(26-Hydroxy-3,6,9,12,15,18,21,24-octaoxahexaicosyl)-3,5-bis(dodecyloxy)benzamide (9)

Similar to **1**, **9** (408 mg, 85%) was synthesized from 3,5-bis(dodecyloxy)benzoic acid (262 mg, 0.54 mmol) and 26-amino-3,6,9,12,15,18,21,24-octaoxa-1-hexaicosanol (310 mg, 0.75 mmol). ^{1}H NMR ($CDCl_3$, 400 MHz), δ 6.93 (s, 1H, –CONH), 6.91 (d, 2H, J = 2.2 Hz, aromatic H), 6.54 (t, 1H, J = 2.2 Hz, aromatic H), 3.95 (t, 4H, J = 6.6 Hz, ArO–CH_2), 3.63 (m, 36H, O–$(CH_2)_2$–O), 3.07 (bs, 1H, –OH), 1.76 (m, 4H, ArOC–CH_2), 1.42 (m, 4H, $ArOC_2$–CH_2), 1.26 (m, 32H, $ArOC_3$–C_8H_{16}), 0.88 (t, 6H, J = 6.8 Hz, –CH_3). ESIMS, found: m/z 908.64, calcd. for $C_{49}H_{91}NO_{12}Na$ ($[M+Na]^+$): 908.64.

2.1.10. N-(8-Hydroxy-3,6-dioxaoctyl)-3,4,5-tris(dodecyloxy)benzamide (10)

Similar to **1**, **10** (387 mg, 90%) was synthesized from 3,4,5-tris(dodecyloxy)benzoic acid (360 mg, 0.53 mmol) and 8-amino-3,6-dioxa-1-octanol (95 mg, 0.63 mmol). ^{1}H NMR ($CDCl_3$, 400 MHz), δ 7.02 (s, 2H, aromatic H), 6.68 (s, 1H, –CONH), 4.01 (t, 6H, J = 6.3 Hz, ArO–CH_2), 3.68 (12H, m, O–$(CH_2)_2$–O), 2.67 (bs, 1H, –OH), 1.78 (m, 6H, ArOC–CH_2), 1.26 (m, 54H, $ArOC_2$–C_9H_{18}), 0.88 (t, 9H, J = 6.9 Hz, –CH_3). ESIMS, found: m/z 828.45, calcd. for $C_{49}H_{91}NO_7Na$ ($[M+Na]^+$): 828.66.

2.1.11. N-(17-Hydroxy-3,6,9,12,15-pentaoxaheptadecyl)-3,4,5-tris(dodecyloxy)benzamide (11)

Similar to **1**, **11** (3.69 g, 88%) was synthesized from 3,4,5-tris(dodecyloxy)benzoic acid (3.02 g, 4.47 mmol) and 17-amino-3,6,9,12,15-pentaoxa-1-heptadecanol (3.77 g, 13.4 mmol). ^{1}H NMR ($CDCl_3$, 400 MHz), δ 7.01 (s, 2H, aromatic H), 6.88 (s, 1H, –CONH), 4.00 (t, 6H, J = 6.5 Hz ArO–CH_2), 3.63 (22H, m, O–$(CH_2)_2$–O), 3.58 (m, 2H, O–CH_2), 2.89 (bs, 1H, –OH), 1.78 (m, 6H, ArOC–CH_2), 1.26 (m, 54H, $ArOC_2$–C_9H_{18}), 0.88 (t, 9H, J = 6.8 Hz, –CH_3). ESIMS, found: m/z 960.66, calcd. for $C_{55}H_{103}NO_{10}Na$ ($[M+Na]^+$): 960.74.

2.1.12. N-(23-Hydroxy-3,6,9,12,15,18,21-heptaoxatriicosyl)-3,4,5-tris(dodecyloxy)benzamide (12)

Similar to **1**, **12** (648 mg, 80%) was synthesized from 3,4,5-tris(dodecyloxy)benzoic acid (535 mg, 0.79 mmol) and 23-amino-3,6,9,12,15,18,21-heptaoxa-1-triicosanol (379 mg, 1.03 mmol). ^{1}H NMR ($CDCl_3$, 400 MHz), δ 7.02 (s, 2H, aromatic H), 6.92 (s, 1H, –CONH), 4.00 (m, 6H, ArO–CH_2), 3.71 (t, 2H, J = 4.1 Hz, O–CH_2), 3.66 (30H, m, O–$(CH_2)_2$–O), 3.01 (bs, 1H, –OH), 1.46 (m, 6H, ArOC–CH_2), 1.29 (m, 54H, $ArOC_2$–C_9H_{18}), 0.88 (t, 9H, J = 7.2 Hz, –CH_3). ESIMS, found: m/z 1048.54, calcd. for $C_{59}H_{111}NO_{12}Na$ ($[M+Na]^+$): 1048.79.

2.2. Critical micelle concentration

A 10^{-5} M aqueous solution of Nile red and sample solutions at concentrations from about 10^{-3} to 10^{-8} M were prepared. The Nile red and the sample solutions were mixed in a ratio of 1:1. The fluorescence of the mixture was measured using a FP750 instrument (JASCO, Tokyo, Japan) at room temperature with excitation at λ = 530 nm and observation at λ = 630 nm.

2.3. Particle size distribution

The concentration of artificial lipids was fixed at 10^{-4} M. Solutions of samples were filtered through a 400 nm pore size polycarbonate membrane using LiposoFast (Avestin, Ottawa, Canada). Particle size distribution was determined by a light scattering method using an Electrophoretic Light Scattering Spectrophotometer, ELS-800 (Otsuka Electronics, Osaka, Japan) at 25 °C.

3. Results and discussion

3,5-Bis- and 3,4,5-tris(dodecyloxy)benzoic acid were prepared from commercially available compounds [1,10]. OEG derivatives of various length were commercially available, and they were converted into monoamino- and diamino-OEG derivatives following a previously reported procedure [11]. The benzoic acid derivatives and OEG amines were condensed to give the target compounds, as shown in Scheme 1.

As shown in Scheme 1, the reaction yields were good to moderate. Since diamino-OEG was condensed without protection, compounds containing a terminal amino group were produced generally in a lower yield compared to the corresponding alcohol derivatives.

The CMC of the artificial lipids was measured by a fluorescent probe method using Nile red [12]. Nile red emits a stronger fluorescence in a hydrophobic environment than in water. The change in fluorescent intensity serves as an index of the formation of a micelle like structure. Fig. 1 shows the fluorescent intensity of Nile red (exited at 530 nm and observed at 630 nm) on an arbitrary scale against the concentration of artificial lipid.

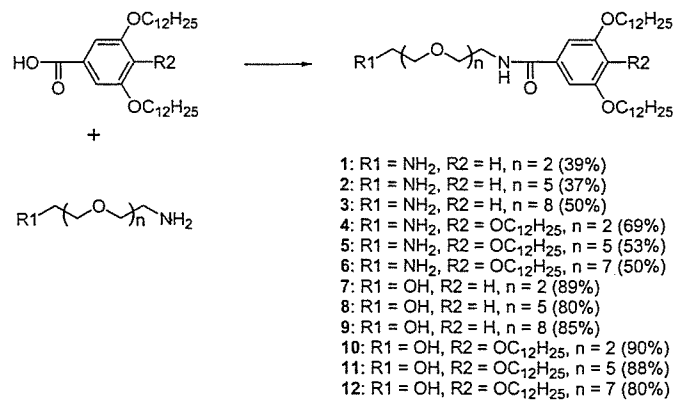

1: R1 = NH_2, R2 = H, n = 2 (39%)
2: R1 = NH_2, R2 = H, n = 5 (37%)
3: R1 = NH_2, R2 = H, n = 8 (50%)
4: R1 = NH_2, R2 = $OC_{12}H_{25}$, n = 2 (69%)
5: R1 = NH_2, R2 = $OC_{12}H_{25}$, n = 5 (53%)
6: R1 = NH_2, R2 = $OC_{12}H_{25}$, n = 7 (50%)
7: R1 = OH, R2 = H, n = 2 (89%)
8: R1 = OH, R2 = H, n = 5 (80%)
9: R1 = OH, R2 = H, n = 8 (85%)
10: R1 = OH, R2 = $OC_{12}H_{25}$, n = 2 (90%)
11: R1 = OH, R2 = $OC_{12}H_{25}$, n = 5 (88%)
12: R1 = OH, R2 = $OC_{12}H_{25}$, n = 7 (80%)

Scheme 1. Synthesis of 12 artificial lipids by condensing amino-OEG and benzoic acid derivatives. The yield of each compound is shown in parentheses.

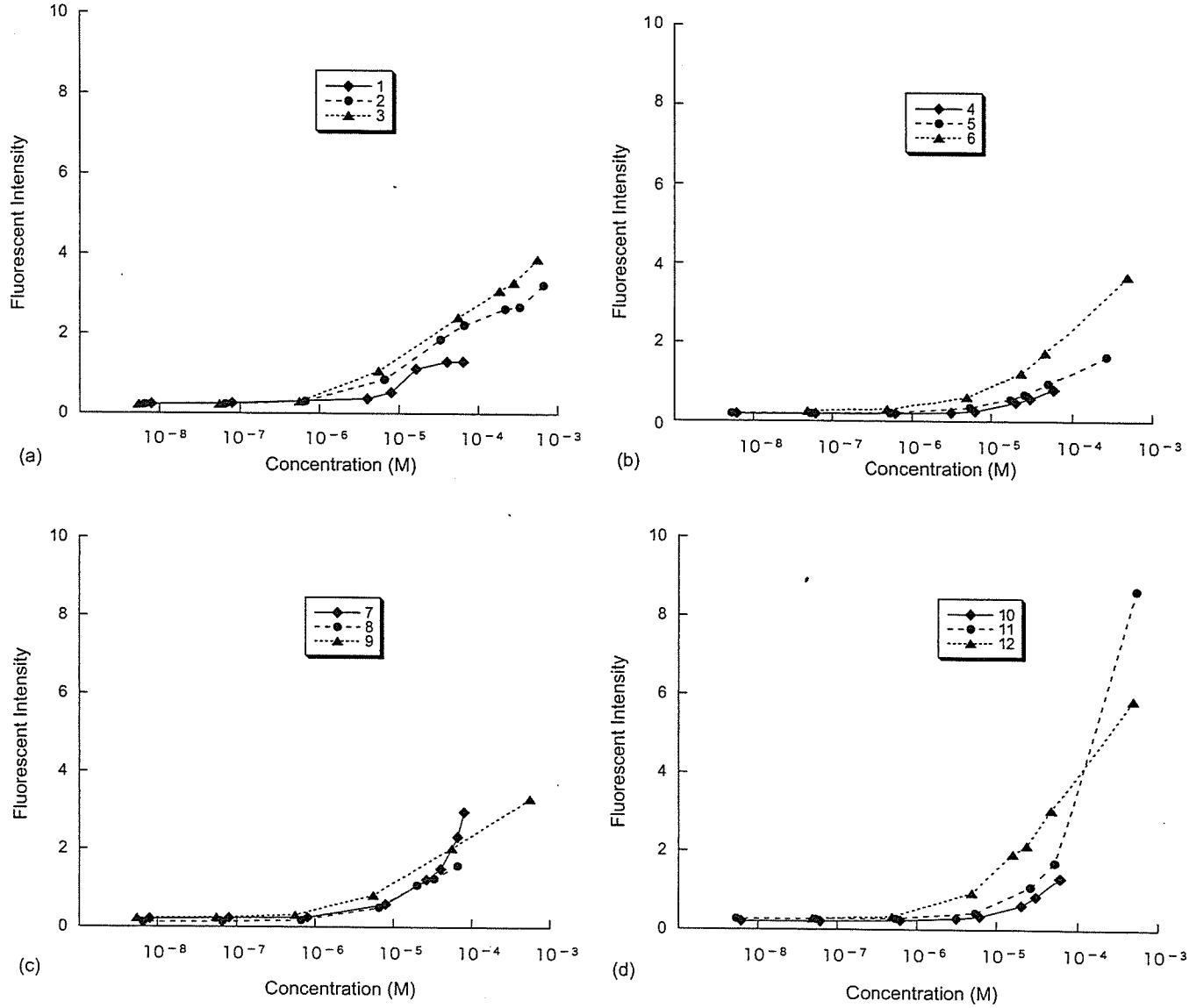

Fig. 1. CMC for the artificial lipids: (a) two alkyl chain amines **1** (diamond), **2** (circle) and **3** (triangle); (b) three alkyl chain amines **4** (diamond), **5** (circle) and **6**; (c) two alkyl chain alcohols **7** (diamond), **8** (circle) and **9** (triangle); (d) three alkyl chain alcohols **10** (diamond), **11** (circle) and **12** (triangle). Nile red was used as a fluorescent probe. The intensity is an arbitrary scale.

Data points for high concentrations of short OEG compounds could not be obtained because of their low solubility.

The CMC for the 3,5-bis(dodecyloxy)benzamide derivatives was $\sim 10^{-6}$ M, and that for the 3,4,5-tris(dodecyloxy)bezamide derivatives was $\sim 10^{-5}$ M. These values are quite low, compared with a conventional surfactant such as sodium dodecyl sulfate ($\sim 10^{-3}$ M) and a commercially available single chain OEG alkyl ether such as $C_{12}E_6$ ($\sim 10^{-4}$ M) [8]. Among the derivatives that contain the same number of dodecyloxy groups, a longer OEG resulted in smaller CMC values. The CMC values for **6** and **12**, in particular, were one order lower than the other 3,4,5-tris(dodecyloxy)bezamide derivatives. No clear difference was found between alcohol and amine derivatives. Only amine **1** showed a higher CMC than the corresponding alcohol **7**, although their low solubility might have obscured the result. A similar monotonous increase in fluorescent intensity was reported for polymer micelles [8], indicating similar micelle structures with a large hydrophobic core.

The particle size distribution of the artificial lipids was analyzed by a light scattering method at a sample concentration of 10^{-4} M at 25 °C. To examine the stability of the micelle like structure, the same sample solution was measured one week later, and these results are summarized in Fig. 2.

Particle size distribution was dependent on the length of the OEG chain, the number of hydrophobic chains, and the nature of the terminal functional group. The short OEG chain compounds, **1**, **7** and **10**, formed insoluble aggregates. The formation of insoluble aggregates was visually discernible, and detected as anomalous large peaks in Fig. 2. Among the compounds with OEG length $n=2$, only **4** remained as dispersion even after 1 week, possibly due in part to the electrostatic repulsion of the amino group. Some of the artificial lipids, especially those with OEG length $n=5$, showed a two peak distribution. When the

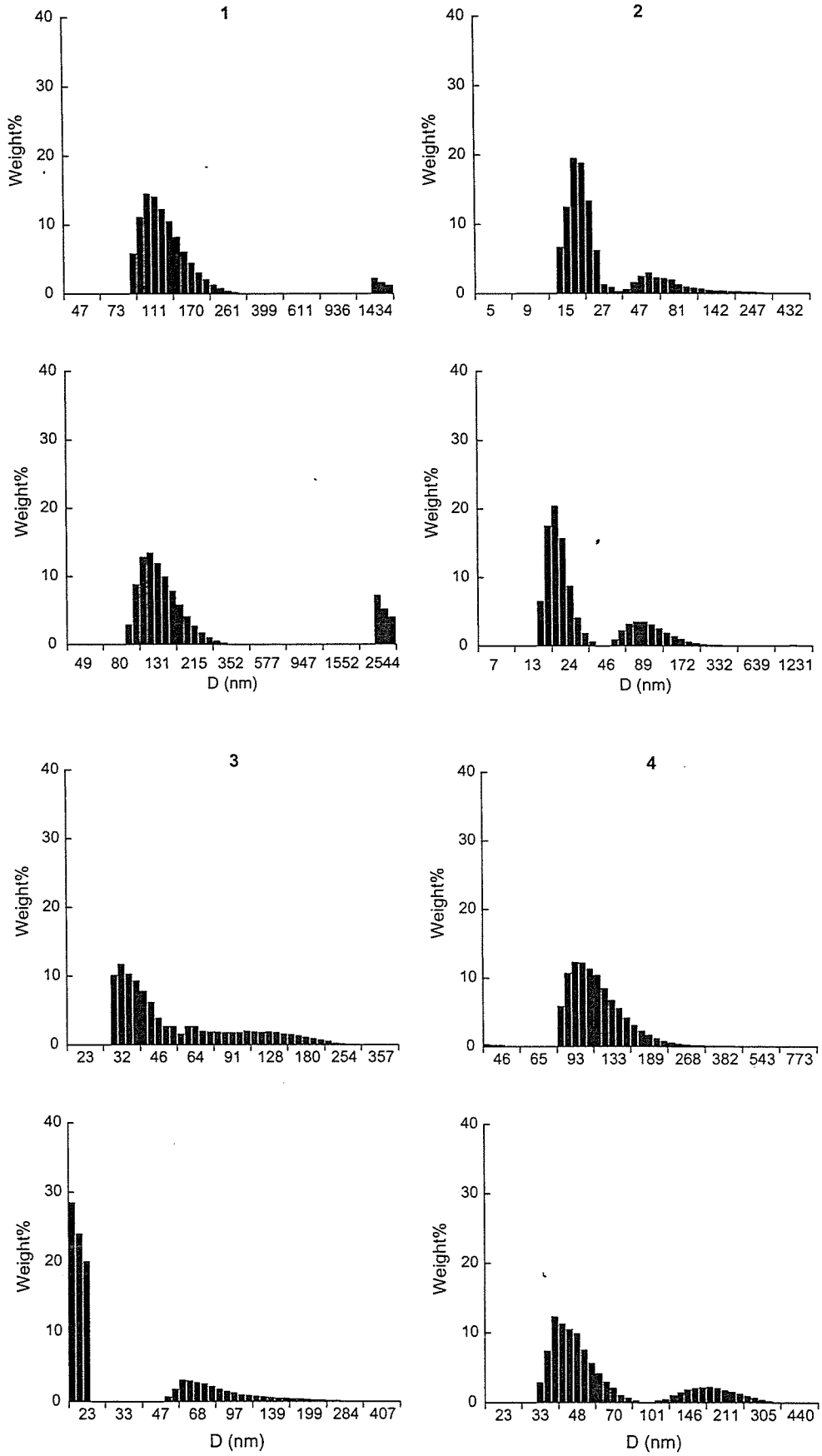

Fig. 2. Particle size distribution of the artificial lipids, determined by a dynamic light scattering method. The number in the figure corresponds to the compound number in Fig. 1. The lower panel for each compound shows the distribution after 1 week. The distribution is shown in wt%.

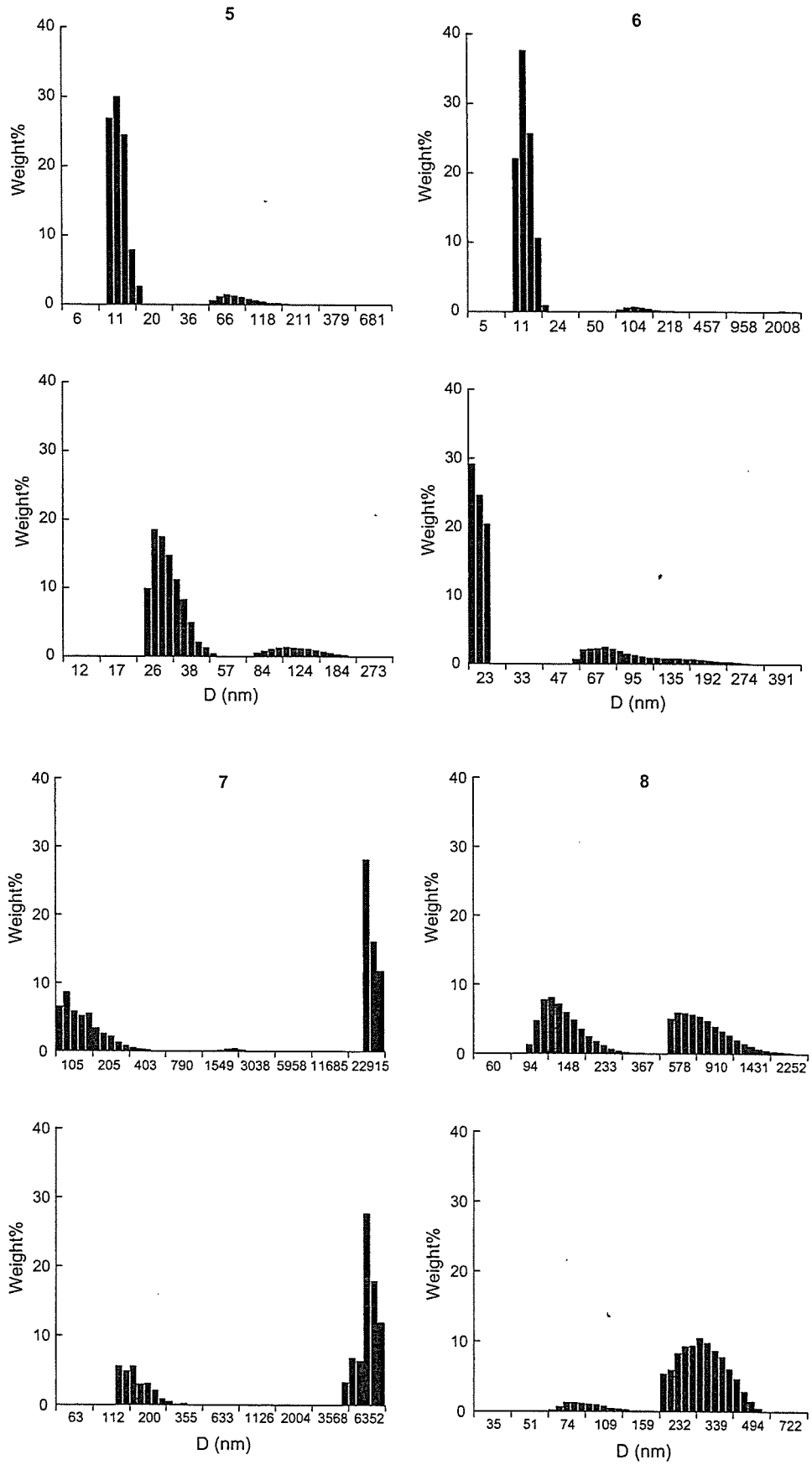

Fig. 2. (*Continued*)

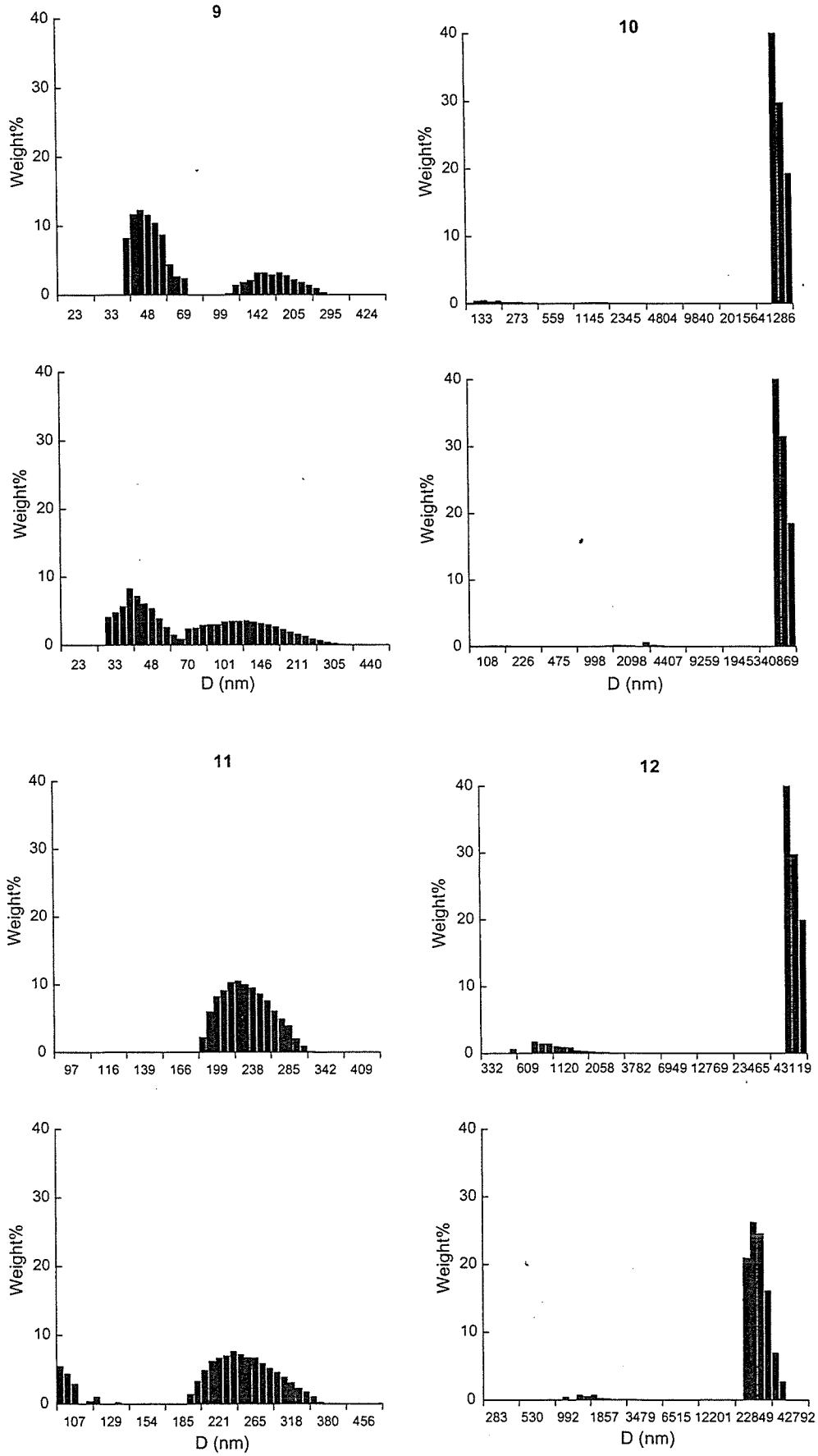

Fig. 2. (*Continued*).

OEG chain became long, the distribution of smaller particles became more prominent. Compound **12** was an exception among the long OEG compounds. It formed very large water-soluble aggregates detected as peaks on the right hand side in Fig. 2. A solution of **12** remained clear even after one week, while that of **1**, **7** or **10** gave visually discernible flocks. The particle size of amine derivative was smaller than that of corresponding alcohol derivatives possibly due to the electrostatic repulsion. The particle size distribution of some of the artificial lipids changed with time, and this was most pronounced in the cases of **4** and **8**, indicating the unstable nature of their nanostructure.

4. Conclusions

Twelve artificial lipids with various OEG lengths containing two or three long alkyl chains were synthesized, and the CMC and particle size distribution of aqueous solutions were determined. Their CMC values were quite low compared with a commercially available single chain OEG alkyl ether, and were mainly dependent on the number of long alkyl chains, though their particle size distribution varied considerably, depending on their structure. Tri(ethylene glycol) derivatives showed a low solubility and tended to aggregate. Hexa(ethylene glycol) derivatives, especially alcohol derivatives **8** and **11**, formed large particles. Octa- or nona(ethylene glycol) derivatives generally gave smaller particles, but **12** was an exception, forming large water-soluble aggregates. Thus, all structural factors, OEG length, the number of alkyl chains, and the terminal functional group, affected the behavior of the artificial lipids in water. Since their particle size or nanostructure may become controllable, these artificial lipids may be useful as bioinert scaffolds for the applications in the field of nanobiotechnology.

References

[1] Y. Azefu, H. Tamiaki, R. Sato, K. Toma, Bioorg. Med. Chem. 10 (2002) 4013–4022.
[2] R. Sato, K. Toma, K. Nomura, M. Takagi, T. Yoshida, Y. Azefu, H. Tamiaki, J. Carbohydr. Chem. 23 (2004) 375–388.
[3] M. Takagi, C. Matsuda, R. Sato, K. Toma, T. Yoshida, J. Biosci. Bioeng. 4 (2002) 437–439.
[4] M. Takagi, K. Nomura, R. Sato, K. Toma, T. Yoshida, J. Artif. Organs 4 (2001) 315–319.
[5] T. Okamoto, M. Takagi, T. Soma, H. Ogawa, M. Kawakami, M. Mukubo, K. Kubo, R. Sato, K. Toma, T. Yoshida, J. Artif. Organs 7 (2004) 194–202.
[6] M. Hara, Y. Takanashi, N. Tuzuki, H. Kawakami, K. Toma, A. Higuchi, Cytotechnology 42 (2003) 13–20.
[7] M. Jonstromer, B. Jonsson, B. Lindman, J. Phys. Chem. 95 (1991) 3293–3300.
[8] S.L. Romsted, J. Yao, Langmuir 12 (1996) 2425–2432.
[9] F. Sterpone, C. Pierleoni, G. Briganti, M. Marchi, Langmuir 20 (2004) 4311–4314.
[10] H. Tamiaki, T. Obata, Y. Azefu, K. Toma, Bull. Chem. Soc. Jpn. 74 (2001) 733–738.
[11] J. Slama, R. Rando, Biochemistry 19 (1980) 4595–4600.
[12] D. Watkins, J. Klimash, Langmuir 13 (1997) 3136–3141.

GENE DELIVERY

ELSEVIER

Available online at www.sciencedirect.com
SCIENCE DIRECT®

Journal of Controlled Release 112 (2006) 362–368

journal of controlled release

www.elsevier.com/locate/jconrel

Biosurfactant MEL-A enhances cellular association and gene transfection by cationic liposome

Saki Igarashi, Yoshiyuki Hattori, Yoshie Maitani *

Institute of Medicinal Chemistry, Hoshi University, Ebara 2-4-41, Shinagawa-ku, Tokyo 142-8501, Japan

Received 28 June 2005; accepted 7 March 2006
Available online 19 April 2006

Abstract

Mannnosylerythritol lipid A (MEL-A), a biosurfactant produced by microorganisms, has many biological activities. To enhance the gene transfection efficiency of a cationic liposome, we prepared a MEL-liposome (MEL-L) composed of 3β-[*N*-(*N'*,*N'*-dimethylaminoethane)-carbamoyl] cholesterol (DC-Chol), dioleoyl phosphatidylethanolamine (DOPE) and MEL-A, and investigated its transfection efficiency in human cervix carcinoma Hela cells. MEL-L was about 40 nm in size, and the MEL-L/plasmid DNA complex (MEL-lipoplex) remained an injectable size (169 nm). MEL-A induced a significantly higher level of gene expression, compared to commercially available Tfx20 and the liposome without MEL-A (Cont-L). Analysis of flow cytometric profiles clearly indicated that the amount of DNA associated with the cells was rapidly increased and sustained by addition of MEL-A to the liposome. Confocal microscopic observation indicated that the MEL-lipoplex distributed widely in the cytoplasm, and the DNA was detected strongly in the cytoplasm and around the nucleus, compared with Cont-L. These results suggested that MEL-A increased gene expression by enhancing the association of the lipoplexes with the cells in serum. MEL-L might prove a remarkable non-viral vector for gene transfection and gene therapy.

Keywords: Biosurfactant; Cationic liposome; DC-Chol; Cellular association; Gene expression

1. Introduction

In gene therapy, the transport and delivery of DNA inside cells are key steps. Viral and non-viral vectors for transferring DNA have been developed intensively. Viral vectors are efficient but have various disadvantages such as immune recognition and potential virus-associated toxicity, including helper virus replication and insertional mutagenesis. In contrast, non-viral vectors are highly attractive due to their excellent safety profile despite their low transgene expression efficiency in comparison to viral vectors. The cationic liposome-mediated transfer of DNA is a particularly promising approach, because of low immunogenicity and toxicity, ease of preparation, and potential applications for active targeting. Therefore, cationic lipids and improved formulations of liposome have been developed for the efficient delivery of DNA to cells [1,2]. Notably, cationic liposomes composed of 3β-[*N*-(*N'*,*N'*-dimethylaminoethane)carbamoyl] cholesterol (DC-Chol) together with dioleoylphosphatidylethanolamine (DOPE) have been reported as an efficient vector for the transfection of DNA into cells [3–5] and in clinical trials [6,7].

Glycolipid biosurfactants (BSs) have received much attention as leading materials for drug-carrying microcapsules and artificial cells, owing to their stabilizing effect on liposomes [8,9]. BSs have numerous advantages, such as lower toxicity, higher biodegradability and unique biological activities. To further improve the transfection efficiency, a BS was used as a component of liposomes, resulting in increased transfection [10]. Mannosylerythritol lipid (MEL) is a BS abundantly produced by the yeast strain *Candida antarctica* T-34 [11]. MEL exhibits excellent surface-activity [12] (i.e., an efficient decrease in surface tension), remarkable cell differentiation and growth inhibition against human leukemia [13], mouse melanoma [3] and PC12 cells [14], and antimicrobial activity particularly against Gram-positive bacteria [13]. One MEL-related compound is MEL-A,

* Corresponding author. Tel./fax: +81 3 5498 5048.
E-mail address: yoshie@hoshi.ac.jp (Y. Maitani).

0168-3659/$ - see front matter © 2006 Elsevier B.V. All rights reserved.
doi:10.1016/j.jconrel.2006.03.003

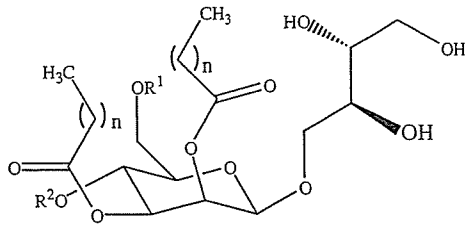

MEL-A; R_1=R_2=Ac

(n=6-10)

Mannosylerythritol lipid A (MEL-A)

Fig. 1. Chemical structure of biosurfactant MEL-A. MEL-A consists of 4-*O*-(di-*O*-acetyl-di-*O*-alkanoyl-β-D-mannopyranosyl)-erythritol esterified two fatty acids and two acetic acids.

which consists of 4,6-di-*O*-acetyl-2,3-di-*O*-alkanoyl-β-D-mannopyranosyl-(1→4)-*O*-erythritol esterified with two fatty acids and two acetic acids (Fig. 1). MEL-A increased remarkably the transfection efficiency of liposomes with a cationic cholesterol derivative such as DC-Chol bearing a tertiary amine head group and cholesteryl-3β-carboxyamindoethylene-*N*-hydroxyethylamine (OH-Chol) bearing a secondary amine head group [10]. The mechanism of gene transfection by MEL-A with OH-Chol/DOPE liposome, but not that with DC-Chol/DOPE liposome, has been clarified [15]. We found that MEL-A added in DC-Chol/DOPE liposomes increased transfection efficiency in serum and did not show a similar mechanism of transfection increased with OH-Chol.

In the present study, we investigated the mechanism by which gene transfection was enhanced by cationic liposomes composed of DC-Chol, DOPE and MEL-A (MEL-L) in Hela cells, measuring the cellular uptake and the intracellular localization of liposome/DNA complexes by flow cytometry and confocal laser scanner microscopy, compared to cationic liposomes without MEL-A (Cont-L). The results suggested that MEL-A enhanced the association of lipoplexes with the cells, delivered it widely into the cytoplasm and increased gene expression.

2. Materials and methods

2.1. Materials

MEL-A and 7-nitrobenz-2-oxa-1,3-diazole (NBD)-labeled MEL-A were supplied by Dr. Kitamoto (National Institute of Advanced Industrial Science and Technology, Tsukuba, Japan). DOPE was obtained from Avanti Polar Lipids Inc. (Alabaster, AL, USA). DC-Chol was purchased from Sigma Chemical Co. (St. Louis, MO, USA). Tfx20 was purchased from Promega (Madison, WI, USA). The Pica gene luciferase assay kit was purchased from Toyo Ink Mfg. Co. Ltd. (Tokyo, Japan). BCA protein assay reagent was purchased from Pierce (Rockford, IL, USA). All other reagents were of analytical grade.

2.2. Preparation of oligonucleotide and plasmid DNA

The FITC-labeled 20-mer randomized oligodeoxynucleotide (5′-CGAGTGCACACGCCTCTCAG-3′, FITC-ODN) was synthesized with a phosphodiester backbone (Sigma Genosys Japan, Hokkaido, Japan). pCMV-luc was constructed using a cDNA fragment (589 bp) coding for a cytomegalovirus (CMV) promoter amplified by PCR with a pEGFP-C1 plasmid (Clontech, CA, USA) containing a green fluorescent protein (GFP) reporter gene under the control of the CMV promoter as a template, and the following CMV promoter-specific primers: CMV promoter forward primer (5′-ATGGTACCTAGTTATTAATAGTAATCAA-3′) and CMV promoter reverse primer (5′-TCAAGCTTGATCTGACGGTTCACTAAAC-3′). The forward and reverse primers, respectively, contained *Kpn*I and *Hind*III restriction sites (underlines). After the amplification, the cDNA was digested with *Kpn*I and *Hind*III and ligated into a *Kpn*I/*Hind*III-digested pGL3-enhancer (Promega, Madison, WI, USA).

A protein-free preparation of the plasmid was purified following alkaline lysis using maxiprep columns (Qiagen, Hilden, Germany).

2.3. Cell culture

A human cervix carcinoma cell line, Hela 229, was supplied by the Department of Virology, Toyama Medical and Pharmaceutical University. The cells were grown in Minimal Essential Medium (MEM, Life Technologies, Inc., Grand Island, NY, USA) supplemented with kanamycin and 5% fetal bovine serum. Cells were grown at 37 °C in a 5% CO_2/air incubator.

2.4. Preparation of liposomes

Two liposomal formulae were used: DC-Chol, DOPE and MEL-A in a 3:2:2 molar ratio for MEL-L; and DC-Chol and DOPE in a 3:2 molar ratio for Cont-L were prepared by a modified ethanol injection method. Briefly, DC-Chol, DOPE and MEL-A were dissolved and mixed in ethanol and the solution was evaporated leaving behind about 2 ml of the solution. Next, a constant volume of water was added to the ethanol solution, and the mixture was evaporated again until only the ethanol was left. After sonication for 15 min in a bath type sonicator, the solution was filtrated through 0.45-μm Millex-HA filters (Millipore, Cork, Ireland) at once for sterilization. The particle size distributions and the ζ-potentials were measured by the dynamic light scattering method and the electrophoresis light scattering method, respectively (ELS-800, Otsuka Electronics Co., Ltd., Osaka, Japan), at 25 °C after the dispersion was diluted to an appropriate volume with water. In 1,1′-dioctadecyl-3, 3, 3′, 3′-tetramethylindocarbocyanine perchlorate (DiI) (Lambda Probes & Diagnostics, Graz, Austria)-labeled liposomes, DiI was incorporated at 0.04 mol% of all the lipids. In NBD-labeled MEL-L, NBD-labeled MEL-A was added at 24% of all the MEL-A.

2.5. Transfection

Cell cultures were prepared by plating cells in a 35-mm culture dish 24 h prior to each experiment. The cells at confluences of 70% in the well were transfected with each lipoplex. Lipoplex at a charge ratio (+/−) of 3/1of cationic lipid to DNA was formed by addition of liposome to DNA (3.8 μl MEL-L (6.9 mg total lipid/ml) or Cont-L (4.8 mg total lipid/ml) suspension in water to 2 μg of DNA, MEL- or Cont-lipoplex) with gentle shaking and leaving at room temperature for 10–15 min. The lipoplexes were diluted with MEM containing 5% serum to a final concentration of 2 μg of DNA per 1 ml of medium, and incubated with the cells for 24 h in the medium. In effect of inhibitor of endocytosis on the transfection activity, the cells were treated with 50 μM chloroquine for 2 h and were then incubated with the lipoplexes for 24 h. The cell toxicity by transfection with the lipoplexes was determined with a WST-8 assay (Dojindo Laboratories, Kumamoto, Japan).

2.6. Luciferase assay

The pCMV-luc plasmid was transfected into cells by MEL-L and Cont-L, respectively. After 24 h of incubation, the cells were washed twice with PBS (pH 7.4) and harvested with 125 μl of cell culture lysis reagent (Toyo Ink, Tokyo, Japan). Luciferase expression was quantified with 10 μl of centrifuged lysate supernatant using a picagene luciferase assay kit (Toyo Ink, Tokyo, Japan) as described previously [16]. Light emission, expressed in counts per second (cps), was normalized to the protein concentration of each sample, determined using BCA protein assay reagent.

2.7. Flow cytometry

The cells were prepared by plating in a 35-mm culture dish 24 h prior to each experiment. Each liposome (3.8 μl) was mixed with 2 μg of FITC-ODN or DiI-labeled liposome mixed with 2 μg of ODN, and then diluted in 1 ml of the medium. The cells were incubated with the lipoplex for 1, 2 and 6 h. After incubation, the dishes were washed 2 times with 1 ml of PBS (pH 7.4) to remove any unbound lipoplexes. The cells were detached with 0.25% trypsin and centrifuged at 1500*g*. The supernatant was discarded and the cells were resuspended with PBS containing 0.1% BSA and 1 mM EDTA. The suspended cells were directly introduced into a FACSCalibur flow cytometry (Becton Dickinson, San Jose, CA, USA) equipped with a 488-nm argon ion laser. Data for 10,000 fluorescent events were obtained by recording forward scatter (FSC), side scatter (SSC), and green (530/30 nm) fluorescence.

2.8. Confocal laser scanning microscopy

Hela cells were prepared by plating cells in a 35-mm culture dish 24 h prior to each experiment. DiI-labeled, NBD-labeled or non-labeled liposome (3.8 μl) was mixed with 2 μg of FITC-ODN or plasmid DNA and then diluted in 1 ml of the medium. After incubation for the periods indicated in the figures, the cells were washed twice with PBS and fixed with 4% formaldehyde in PBS for 15 min at room temperature. For staining the nucleus, the fixed cells were washed with PBS and incubated with 0.5 mg/ml of RNase in PBS for 20 min at 37 °C. Subsequently, the cells were washed with PBS and incubated with propidium iodide (PI) for 15 min at room temperature. Examinations were performed with a Radiance 2100 confocal laser-scanning microscope (BioRad, CA, USA) as previously described [16].

2.9. Statistical analysis

The statistical significance of the data was evaluated with Student's *t*-test. A p value of 0.05 or less was considered significant.

3. Results and discussion

3.1. Preparation and characterization of MEL-L and Cont-L

The success of gene therapy is largely dependent on the development of vectors as DNA carriers. Cationic liposomes composed of DC-Chol as a cationic lipid and DOPE as a helper lipid are generally used. A molar ratio of 3:2 has been used for DC-Chol /DOPE [5]. In a preliminary study, the addition of MEL-A to DC-Chol /DOPE liposomes increased transfection efficiency in serum, and the ratio of MEL-A to DC-Chol /DOPE liposome was optimized at a molar ratio of 3:2:2 (DC-Chol, DOPE and MEL-A). Therefore, in this study, we prepared two kinds of liposomes; Cont-L consisting of DC-Chol and DOPE at a molar ratio of 3:2 and MEL-L containing 28 mol% MEL-A in a Cont-L formulation. MEL-L and Cont-L were about 43 nm and 156 nm in size, and the lipoplexes about 169 nm and 265 nm in size, respectively (Table 1). Although the concentration of MEL-A and the method used to prepare the liposomes were not the same as those reported by Inoh et al. [10], our observation was consistent with their finding that the addition of MEL-A to liposomes makes them smaller. This suggested that MEL-A kept liposomes small via the biosurfactant's effect.

3.2. Effects of MEL-L on transfection efficiency

Next, we compared the efficiency of transfection into Hela cells between MEL-L, Cont-L and the commercially available transfection reagent Tfx20 in the presence of 5% serum (Fig. 2). MEL-L showed significantly greater transfection activity than

Table 1
Formulation of liposomes

Liposome	Formulation (molar ratio)	Particle size[a] (nm)	ζ-potential (mV)	Lipoplex size[b] (nm)
MEL-L	DC-Chol/DOPE/MEL=3/2/2	43.4±2.8	52.9±2.0	168.6±3.7
Cont-L	DC-Chol/DOPE=3/2	156.4±2.4	70.5±1.2	265.3±101.4

[a] In water.
[b] A change ratio (+/−) of 3/1 in water.

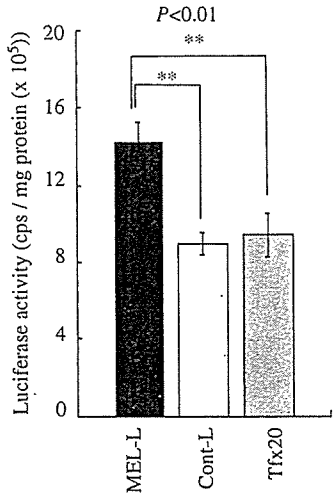

Fig. 2. Effect of MEL-A on transfection efficiency of MEL-L, Cont-L and Tfx20 in Hela cells. Lipoplexes were diluted in medium with serum to a final concentration of 2 μg of DNA in 1 ml of medium per well, and each cell was incubated for 24 h. The charge ratio (+/−) of liposome to plasmid DNA was 3:1. Each result represents the mean±S.D. (n=3).

Cont-L and Tfx20. This suggested that MEL-A enhanced the transfection efficiency of the DC-Chol/DOPE liposome. We also confirmed that MEL-L had no toxicity when the MEL-lipoplex was incubated with Hela cells at the dose used (data not shown). These results were consisted with the finding that cationic liposomes containing MEL-A promoted the efficiency of gene transfection into mammalian cultured cells although MEL-A itself did not increase transfection efficiency [15]. The effect on transfection efficiency might be because MEL-A minimized the aggregation induced by DNA and reduced particle size [10,17].

3.3. Localization of liposome and DNA transfected into Hela cells

To investigate the intracellular localization of the MEL-lipoplex, we prepared lipoplexes of either DiI-labeled MEL-L or Cont-L with FITC-ODN and transfected them into Hela cells (Fig. 3). After 2 or 24 h of incubation, the intracellular localization of the DiI-labeled liposome and FITC-labeled DNA were confirmed by changing the Z-axis of the observed area

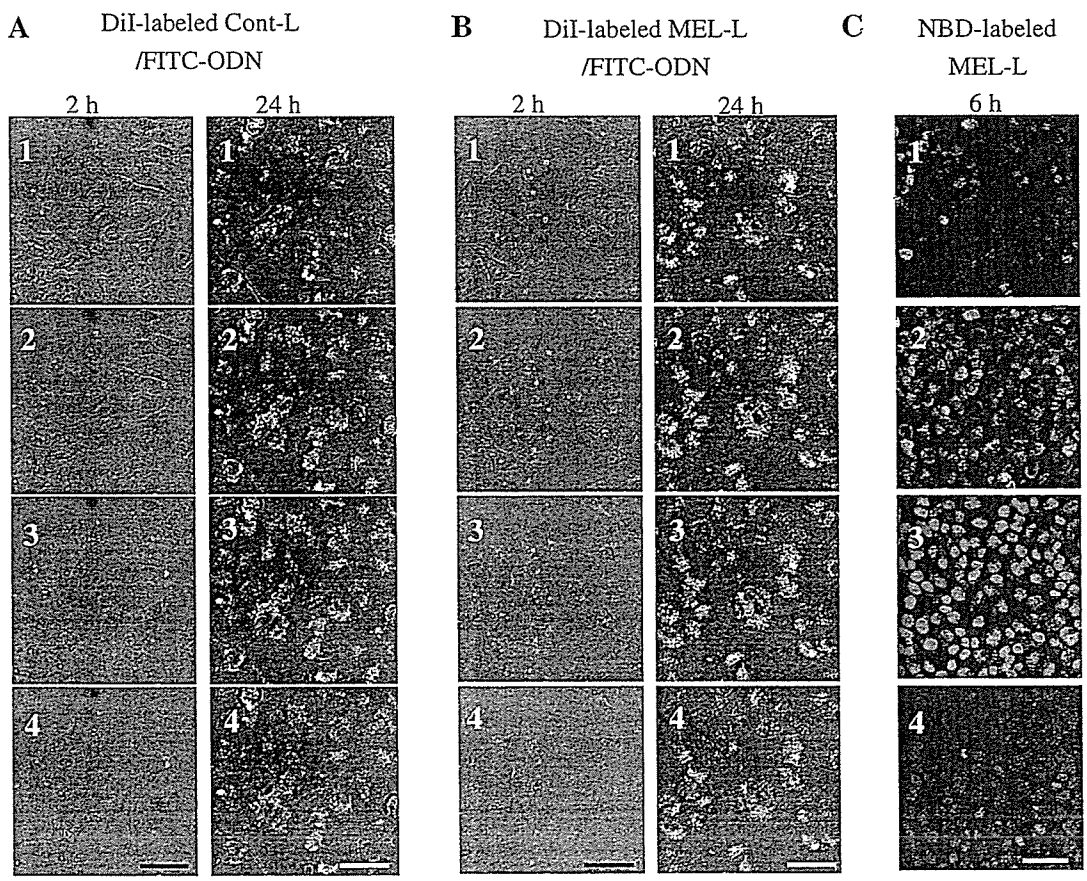

Fig. 3. The localization of lipoplexes of DiI-labeled liposome and FITC-ODN at 2 and 24 h after incubation (A and B). FITC-ODN was mixed with DiI-labeled Cont-L (A) and MEL-L (B), respectively. The localization of lipoplexes of MEL-L with NBD-labeled MEL-A and plasmid DNA at 6 h after incubation (C). Plasmid DNA was mixed with NBD-labeled MEL-L. The lipoplexes were transfected into Hela cells, and observed under a confocal laser microscope by changing the Z-axis. Images 1–4 represent regular intervals of 3 μm on the Z-axis from bottom to top of cells, respectively. In A and B, the red signals show the location of the liposome, and the green signals, that of the FITC-ODN. In C, the red signals show the location of the nucleus, and the green signals, that of the MEL-A. Scale bar=50 μm.

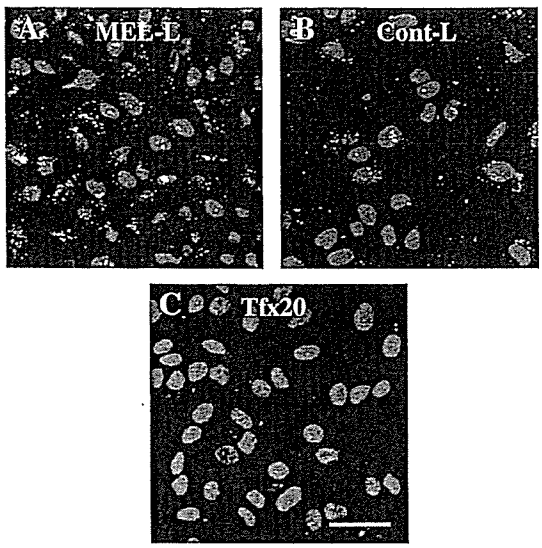

Fig. 4. Intracellular distribution of FITC-ODN by liposomes in Hela cells. FITC-ODN was transfected by MEL-L (A), Cont-L (B) and Tfx20 (C), respectively, into Hela cells. After 6 h of incubation, nuclei were stained by PI, and the cells were examined under a fluorescent microscope using a filter for green-fluorescence (FITC-ODN) and red-fluorescence (nucleus). Scale bar=50 μm.

with 3 μm. DiI-fluorescence was weakly detected in the cytoplasm at 2 h incubation with MEL-L (Fig. 3B), but hardly detected with Cont-L (Fig. 3A). This indicated that MEL-L was rapidly internalized into the cells. At 24 h, DiI-fluorescence and FITC-fluorescence in both MEL-L and Cont-L were widely observed in the cytoplasm.

To confirm the distribution of the DiI-fluorescence of MEL-L by MEL-A, we prepared lipoplexes using NBD-labeled MEL-L with NBD-labeled MEL-A and transfected them into Hela cells. After 6 h of incubation, NBD-labeled MEL-A was widely observed in the cytoplasm but not detected in the nucleus (Fig. 3C). This localization was similar to that of DiI-labeled MEL-L (Fig. 3B) and suggested that MEL-A of MEL-L enhanced the association of MEL-lipoplex with the cells and induced the distribution of liposome and DNA into the cytoplasm. This might explain the enhancement of transfection efficiency by MEL-A. Inoh et al. reported that lipoplexes containing MEL-A and OH-Chol were temporarily located on the plasma membrane of target cells [15]. However, our results showed that MEL-A was located throughout the cytoplasm. We cannot explain this discrepancy, but the difference in cationic lipids might affect the distribution of MEL-L in the target cell.

To confirm the localization of DNA in the cells, lipoplexes of FITC-ODN were formed with MEL-L, Cont-L and Tfx20, respectively, and transfected into Hela cells. The fluorescence of FITC-ODN in the cells was more strongly observed in MEL-L than in Cont-L at 6 h of incubation (Fig. 4A and B). In MEL-L, FITC-ODN was distributed around the nucleus and cytoplasm, but in Cont-L, it was mostly localized to the cytoplasm. In Tfx20, little fluorescence was observed (Fig. 4C). This suggested that MEL-L could deliver DNA into the cytoplasm and nucleus better than Cont-L or Tfx20.

3.4. Association of MEL-, Cont- and, Tfx20-lipoplexes with the cells

To compare the cellular association of the DNA transfected by MEL-L, Cont-L and Tfx20, respectively, we examined the

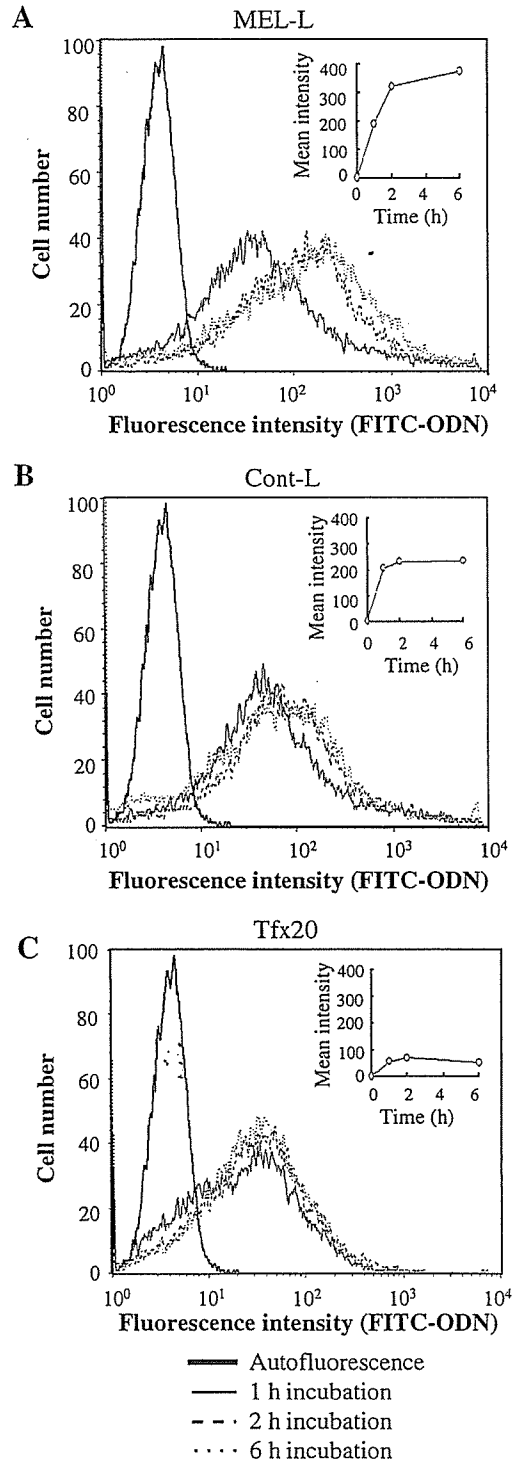

Fig. 5. The cellular association with lipoplexes of FITC-ODN. The kinetics of the cellular association of FITC-ODN transfected with MEL-L (A), Cont-L (B) and Tfx20 (C) was evaluated by flow cytometry. Each lipoplex was incubated with cells for 1, 2 and 6 h.